DOE/PC/95101--74

PSI-1245

TOXIC SUBSTANCES FROM COAL COMBUSTION --
A COMPREHENSIVE ASSESSMENT

Quarterly Report No. 4
for the period
1 July 1996 - 30 September 1996

Dr. L.E. Bool III and Dr. C.L. Senior
Physical Sciences Inc.
20 New England Business Center
Andover, MA 01810-1077

Prof. F. Huggins, Prof. G.P. Huffman, and Prof. N. Shah
University of Kentucky
341 Bowman Hall
Lexington, KY 40506-0059

Prof. J.O.L. Wendt and Prof. T.W. Peterson
University of Arizona
Geology Building Room 1008B
Tucson, AZ 85721

Prof. A.F. Sarofim, Prof. I. Olmez, and Mr. Taofang Zeng
Massachusetts Institute of Technology
Cambridge, MA 02139

Dr. S. Crowley and Dr. R. Finkelman
U.S. Geological Survey
National Center, MS-956
Reston, VA 22092

RECEIVED
USDOE/PETC
'95 NOV -4 AM 11:06
ACQUISITION & ASSISTANCE DIV.

MASTER

October 1996

PSI
PHYSICAL SCIENCES INC.

DISCLAIMER

Portions of this document may be illegible
in electronic image products.   Images are
produced from the best available original
document.

DISCLAIMER

TABLE OF CONTENTS

LIST OF FIGURES

LIST OF FIGURES (Continued)

LIST OF TABLES

ABSTRACT

The Clean Air Act Amendments of 1990 identify a number of hazardous air pollutants (HAPs) as candidates for regulation. Should regulations be imposed on HAP emissions from coal-fired power plants, a sound understanding of the fundamental principles controlling the formation and partitioning of toxic species during coal combustion will be needed. With support from the Pittsburgh Energy Technology Center (PETC), the Electric Power Research Institute (EPRI), and VTT (Finland), Physical Sciences Inc. (PSI) has teamed with researchers from USGS, MIT, the University of Arizona (UA), the University of Kentucky (UKy), the University of Connecticut, and Princeton University to develop a broadly applicable emissions model useful to regulators and utility planners. The new Toxics Partitioning Engineering Model (ToPEM) *will* be applicable to *all* combustion conditions including new fuels and coal blends, low-NO$_x$ combustion systems, and new power generation plants. Development of ToPEM will be based on PSI's existing Engineering Model for Ash Formation (EMAF). Extensive coal characterization and laboratory work has begun in order to develop and test new sub-models. Trace element concentrations in the Pittsburgh, Elkhorn/Hazard, and Illinois No. 6 coals, and in size/density fractions of these coals, were completed. Coal characterization in the past quarter also included direct identification of the modes of occurrence of various trace inorganic species in coal and ash using unique analytical techniques such as XAFS analysis and selective leaching. Combustion testing of these two coals was begun and preliminary data obtained on trace element vaporization in the combustion zone. Modeling efforts in the past quarter include the development on a preliminary model to assess mercury speciation in combustion systems.

SECTION 1

EXECUTIVE SUMMARY

1. EXECUTIVE SUMMARY

The technical objectives of this project are:

a. To identify the effect of the mode-of-occurrence of toxic elements in coal on the partitioning of these elements among vapor, submicron fume, and fly ash during the combustion of pulverized coal,

b. To identify the mechanisms governing the post-vaporization interaction of toxic elements and major minerals or unburnt char,

c. To determine the effect of combustion environment (i.e., fuel rich or fuel lean) on the partitioning of trace elements between vapor, submicron fume, and fly ash during the combustion of pulverized coal,

d. To model the partitioning of toxic elements between various chemical species in the vapor phase and between the vapor phase and complex aluminosilicate melts,

e. To develop a frame work for incorporating the results of the program into the Engineering Model for Ash Formation (EMAF).

A description of the work plan for accomplishing these objectives is presented in Section 2.1 of this report.

The work discussed in this report highlights the accomplishments of the fourth quarter of this program. These accomplishments include trace element analysis of the third program coal, the Illinois No. 6, and size and density segregated samples of all three coals by Nuetron Activation Analysis (NAA). These results are complemented by analyses by the USGS using ICP-MS and other techniques to measure the trace element concentrations in all three program coals distributed to date. XAFS and microprobe analysis were used to determine the forms of occurrence of various trace elements. Combustion experiments were performed at two different scales to begin to explore vaporization of trace elements in the combustion zone.

Specifically, the coal particle size distributions were found to be very similar for all three program coals obtained to date. In addition, trace element concentration measurements in each coal by NAA and other techniques were completed in the last quarter and are described in Section 3.2. In general the trace element concentrations determined from NAA were comparable to those determined by other methods. Trace element concentrations were also measured, by NAA, for selected size and density fractions of the three coals. In general the elemental concentrations were found to be similar in the various fractions. However, a few elements (particularly arsenic) were found to be enriched in the higher density fractions for most coals.

X-ray absorption fine structure (XAFS) analysis was utilized to measure the forms of occurrence of selected trace elements in the three coals. For example, this technique was used to show that arsenic was primarily in the form of arsenical pyrite in the Pittsburgh coal, whereas

approximately half of the arsenic was in the form of arsenate in the Elkhorn/Hazard coal. The concentration of arsenic in pyrite is higher for the Elkhorn/Hazard coal than in the Pittsburgh and Illinois No. 6 coals. XAFS spectra for other elements have been collected and are currently being analyzed.

Combustion experiments in the past quarter focussed primarily on the vaporization of trace elements in the combustion zone. Size and density fractions of all three coals were burned in the MIT drop tube furnace and size segregated ash samples were collected. Utility grind samples of the Pittsburgh and Elkhorn/Hazard coals were burned under slightly fuel rich conditions in the PSI entrained flow reactor (EFR). In all experiments antimony, arsenic, and selenium were enriched in the fine (<1 μm) size -- suggesting vaporization of these elements in the flame zone. The MIT experiments also indicated significant vaporization of other species such ash zinc and iron. For some elements, such as antimony and arsenic, the MIT results indicate that the fractional vaporization was higher in the high density fractions of the coal. In all cases the degree of vaporization was substantially higher in the MIT experiments than in the PSI experiments. This difference is likely due to differences in the combustion environment in the two reactors as the MIT uses extremely fuel lean conditions, while the PSI experiments utilized slightly fuel rich conditions.

Preliminary examination of the literature data, and equilibrium calculations, were used to explore modeling mercury speciation in boilers. Equilibrium suggests that all mercury should be oxidized at stack temperatures, while the measured values suggest only 50 to 90% of the mercury is oxidized. Based on this discrepancy, a hypothesis was proposed for mercury speciation in coal combustion flue gas which states that the Hg equilibrium is frozen below some temperature between 725 and 975 K. The preliminary modeling supported this hypothesis, but further validation is required.

1-4

SECTION 2

INTRODUCTION AND PROGRAM OVERVIEW

2. INTRODUCTION AND PROGRAM OVERVIEW

2.1   Introduction

Before electric utilities can plan or implement emissions minimization strategies for hazardous pollutants, they must have an accurate and site-specific means of predicting emissions in all effluent streams for the broad range of fuels and operating conditions commonly utilized. Development of a broadly applicable emissions model useful to utility planners first requires a sound understanding of the fundamental principles controlling the formation and partitioning of toxic species during coal combustion (specifically in Phase I, As, Se, Cr, and possibly Hg). PSI and its team members will achieve this objective through the development of an "Engineering Model" that accurately predicts the formation and partitioning of toxic species as a result of coal combustion. The "Toxics Partitioning Engineering Model" (ToPEM) will be applicable to all conditions including new fuels or blends, low-NO_x combustion systems, and new power systems being advanced by DOE in the Combustion 2000 program.

Based on a goal of developing and delivering this ToPEM model, a 5-year research program was proposed. This program is divided into a 2-year Phase I program and a 3-year Phase II program. The objective of the ongoing Phase I program is to develop an experimental and conceptual framework for the behavior of selected trace elements (arsenic, selenium, chromium, and mercury) in combustion systems. This Phase I objective will be achieved by a team of researchers from MIT, UA, UKy, Princeton University, the University of Connecticut, and PSI. Model development and commercialization will be carried out by PSI.

Our general approach to the development of the ToPEM model is to break the process for toxic formation into sub-processes, each of which will be addressed by team members who are experts in the area. Ultimately, this will result in new sub-models which will be added to the existing Engineering Model for Ash Formation (EMAF) to create ToPEM. Figure 2-1 illustrates the relationship between the elements of the Phase I Work Breakdown Structure and the sub-processes. Each of the areas identified in the figure will be addressed in the Phase I program as described below.

2.2   Program Overview

2.2.1   Forms of Occurrence of Trace Elements in Coal

One of the most important questions to be answered in the program as a whole is whether the form of a particular element in the coal affects its form of emission at the end of the process. The answer to this question will determine the shape of the sub-models that must be developed in this program. Thus, a detailed understanding of the forms of individual trace elements in coal provides a foundation for much of the rest of the program. Key issues that will be addressed in Phase I are the specific mineral associations of individual elements and the relationship between trace metal form and "standard" analyses.
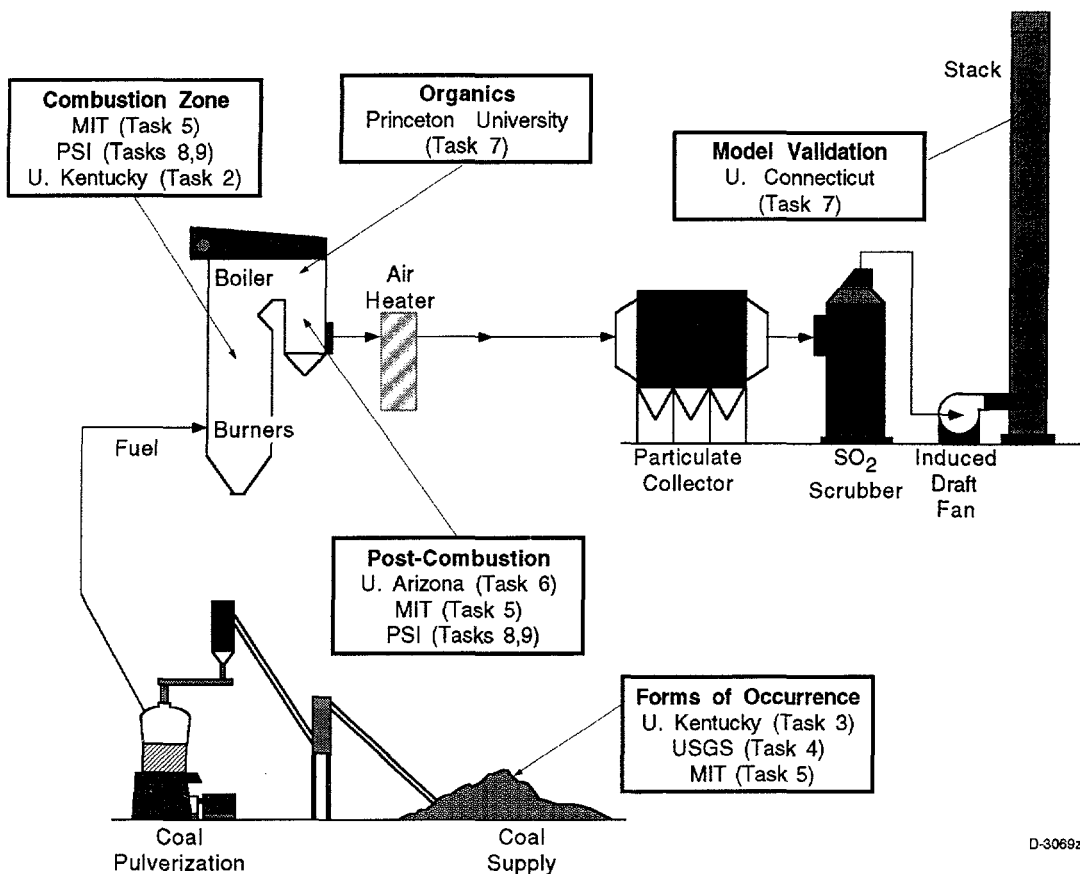
Figure 2-1. Project organization.

Because of the importance of elemental form (e.g., sulfate versus silicate mineral) on partitioning, it is critical that coals representing a broad range of elemental forms be examined in this program. In Task 2 we will select and acquire a total of four coals for study in this program. The coals chosen will (1) represent a broad range of elemental forms of occurrence; (2) represent the major coal ranks and commercial coal seams used for pulverized coal (pc) power generation in the US; and (3) include "future fuels" such as blends and beneficiated coals. Once selected, fresh coal samples will be acquired and distributed to team members. These samples will be subjected to ultimate, proximate, and ASTM ash analysis. Coal samples will be analyzed for trace element concentrations by instrumental neutron activation analysis (INAA) at the MIT Nuclear Reactor Laboratory (Task 5).

Advanced analytical techniques such as Mössbauer spectroscopy and CCSEM will be used by UKy (Task 3) to determine the major mineral species present in the program coals and the combustion generated ash. This analysis will provide important insight on the minerals present in the coal, how they interact during the combustion process, and how this interaction may affect the partitioning of toxic elements.

Another important issue is the form-of-occurrence of the trace elements in the coal. In this task the mode of occurrence of As, Cr, and Se will be determined by combining XAFS and the Mössbauer/CCSEM derived data discussed above. Hg will also be evaluated. Other less

2-4

critical trace elements (Mn, Ni, Zn, Pb, U, etc.) may also be evaluated, especially if their abundance is unusually high in any of the program coals. In addition, the form-of-occurrence of Cl and S in coals and chars will be investigated.

As a complement to the time-intensive XAFS analysis mentioned above, a unique protocol developed by USGS will be used in Task 4 to analyze selected raw coal, and size and density segregated coal, samples for trace element forms of occurrence. This protocol combines low temperature (< 200°C) ashing, chemical analysis, x-ray diffraction, coal segregation via flotation, ammonium acetate and selected acid leaching, electron microbeam measurements, and low and moderate temperature heating tests to determine the forms of elements in coal. Because of the unique combination of existing testing and analytical facilities available at USGS, the work will be conducted at USGS laboratories. In addition, a relatively new technique, synchrotron radiation x-ray fluorescence microscopy (SRXFM), available at the National Synchrotron Light Source, will be tested for application in this area by UKy (Task 3). This technique uses x-ray fluorescence excited by a focussed synchrotron x-ray beam for imaging and compositional analysis. The x-ray yield obtained from a given element is orders of magnitude greater than that possible in an electron microscope or microprobe; hence, its sensitivity to trace element modes is much better, particularly for modes of occurrence involving highly dispersed elements

2.2.2 Combustion Zone Transformations

The effect of coal type and combustion conditions on the emission of the toxic trace elements will be investigated using the MIT laminar-flow drop tube reactor (Task 5). The fundamental mechanisms of toxic species formation and partitioning will be determined from careful examination of the ash formed under a variety of combustion conditions. Measurements will be made of the partitioning of the trace elements in the four coals as a function of temperature and equivalence ratio. These measurements will provide the baseline data on the fraction vaporized for the different elements to be studied in greater detail in Phase II of the program. Individual size-segregated ash samples (collected with a cascade impactor) will then be analyzed by INAA for total composition, Auger and STEM for surface composition, TEM and SEM for particle morphology, and possibly water washing and/or chemical leaching to determine the solubility of selected trace elements in the ash samples. Samples will also be submitted to UK for chemical species analysis by XAFS and other techniques.

PSI will perform a detailed experimental study to determine the fundamental behavior of toxic species during combustion, including low NO_x conditions (Task 8). The work will use the PSI Entrained Flow Reactor (EFR) that has been used in many previous combustion studies on mineral matter transformations during pc combustion. This reactor is on a scale intermediate between the bench top apparatus to be used by other team members (UA, MIT) and the UA laboratory-scale combustor. Therefore the combustor will yield a better understanding of the overall behavior of toxic species while avoiding some of the confounding influences related to self-sustained combustion in the larger furnace. Utility-grind samples of the program coals will be burned under three different stoichiometric ratios, and two temperatures. Size segregated ash samples, and carbon filter samples will be collected. Ash samples collected during the

combustion experiments will be analyzed by INAA and other techniques at MIT. By performing an elemental analysis on the size classified ash samples, we will identify the major mechanisms (e.g., vaporization and condensation) that govern the behavior of specific toxic species during the combustion process -- especially under reducing conditions.

2.2.3 Post-Combustion Transformations

The goal of this task is an increased understanding of the transformations of selected metals as the flue gases cool following the high temperature combustion zone. Experiments will be performed on two very different scales at UA. In addition, PSI will perform thermodynamic equilibrium calculations and make measurements of submicron aerosol size and composition from the large self-sustained combustor (Task 8, 9).

At the small scale, UA will conduct experiments to explore the fundamental kinetics and mechanisms for metal vaporization and metal vapor-mineral interactions. Metal vapor-mineral interactions will be studied in this task using thermogravimetric analysis (TGA). The primary experimental parameters to be studied are temperature, gas composition (particularly the concentration of the metal species in the gas phase), the composition of the sorbent (char, silica, alumino-silicate, etc.), sorbent particle size and porosity, and exposure time (residence time). The primary properties that will be analyzed are the concentration of toxic trace metals in the particles as functions of time, the final chemical form of the trace metal, the leachability of the trace metal in the final particles, and if possible, the distribution of metal in the particles.

On a larger scale, UA will determine how both coal composition, detailed mineralogy and combustion conditions (including low NO_x conditions) govern the fate of toxic metals under practical time/temperature, self sustained, yet still aerodynamically well defined, pulverized coal combustion conditions. Other tasks focus, one at a time, on individual aspects of toxic metal partitioning. In this task, experiments are performed with time-temperature profiles similar to those in pc combustors. Therefore, the hypothesis derived from the smaller scale facilities can be tested under 'real world' conditions to determine the dominant mechanisms for trace element partitioning. Results from this portion of the project, together with the other portions, will lead to a quantitative model that will predict the fate of all toxic species as functions of coal quality and combustion configurations.

Select coals will be burned in the UA self-sustained combustor under premixed conditions where all the coal is mixed with all the air prior to combustion. The baseline tests will employ the naturally occurring temperature profile for each coal at a stoichiometric ratio of 1.2. Samples will be withdrawn at the exhaust port. Complete impactor samples will be collected and analyzed for each toxic metal (11 as listed in the CAAA plus U and Th) plus major elements. This will yield the particle size segregated toxic metal composition, which can be compared to data obtained form other tasks of this program. This data will then be examined to determine particle size dependence in order to infer possible mechanisms governing the fate of each metal.

2.2.4 Organic Emissions

Some organic emissions associated with coal combustors can have deleterious effects on the environment and/or human health. It is therefore very important (1) to know the identities, quantities, and toxicities of the organic species released from coal combustion systems and (2) to understand the chemical and physical processes that govern these species' formation, destruction, and release. Organic emissions data from the DOE Air Toxics and EPRI PISCES programs have the potential of benefitting the evaluation of the problem of organic emissions from coal combustion. In Task 7, Princeton University will conduct a critical review of the available field data, focusing on (1) the appropriateness, thoroughness, and reliability of the experimental techniques employed, (2) comparison with previously published emissions data, and (3) the implications of the results, to similarly evaluate comparable data available from other countries, particularly Europe and Australia; review emerging technical literature on coal pyrolysis and combustion processes that affect organic emissions; to stay abreast of new results in the toxicity literature, relating to organic emissions from coal; and to communicate regularly with the other principal investigators of the air toxics team so that all will be cognizant of the ties between the organic and inorganic air toxics issues.

It is expected that the above efforts of analysis and literature review will lead to (1) comprehensive understanding of what is currently known about organic emissions from coal and (2) identification of the important questions that may still need to be addressed in future research.

2.2.5 Model Validation

Also under Task 7, the University of Connecticut will conduct a preliminary review of the relevant field data on inorganic emissions. In Phase I we will use the field data to focus the experimental program and to validate the models we will develop in Phase II. The Phase I effort focuses on data from the following sources:

- EPRI PISCES
- DOE Program
- VTT (Finland)
- KEMA (Netherlands)

Important issues to be addressed when reviewing these data include mass balance closure, methods of analysis and sample collection, effect of APCD, effect of bulk coal ash chemistry, particle size distribution, and speciation of Hg.

2.2.6 Model Development

PSI will use its silicate equilibrium model accounts for the *non-ideal* behavior of multi component silicate solutions in combination with its trace element database to calculate Cr and As partitioning. These results will be compared with laboratory data generated under Tasks 5.1, 6.1, 6.2, and 8, and inorganic species field data reviewed as part of Task 7. These calculations may be repeated for Se and/or other elements if experimental data warrant interpretation of vaporization under conditions where silicate chemistry is dominant.

SECTION 3

RESULTS AND DISCUSSION

3. RESULTS AND DISCUSSION

3.1   Program Management (PSI)

A program review meeting was held on September 5 in Pittsburgh. Each Principal Investigator presented current work in progress and plans (which are summarized elsewhere in this report). During the meeting there were many suggestions for steps to clarify the experiments or improve the value of the data. These are discussed below.

We have yet to demonstrate that oxidation of the minerals in coal alters the behavior of toxic metals during combustion. However, we feel that for some metals, particularly those associated with pyrite, the degree of oxidation may determine the split between submicron fume and residual ash. We discussed a controlled oxidation experiment, in which oxidation is accelerated in the laboratory. The degree of oxidation can be tracked by Mössbauer; XAFS can be used to look at oxidation of As. When significant oxidation has been shown to occur, PSI can do combustion experiments to determine the degree of vaporization.

It was noted that mild heating (ca. 102° C) of coal seems to drive off part of the mercury. We discussed whether pulverization would affect the mercury content of the program coals. Would the mercury volatilized during pulverization just re-adsorb on the carbon? One test suggested was to analyze an Illinois 6 sample that has not been pulverized for Hg content.

There was a lot of discussion on mercury speciation in the flue gas. Ash from the Pittsburgh coal has been observed to have catalytic properties for oxidation of Hg to $HgCl_2$. Does the ash and/or char promote formation of Cl_2 from HCl (since the oxidation of Hg by Cl_2 has been observed to be much faster than by HCl)? Or, does the ash and/or char adsorb Hg which is then converted to $HgCl_2$? We might try adding either Cl_2 or HCl in the U of A sorbent experiments to look at the effect of chlorine speciation on mercury-char interactions.

3.2   Coal Characterization (UKy, USGS, MIT)

In order to fully understand and predict the behavior of trace elements during combustion it is extremely important to know the forms in which these elements exist in coal. For this reason a great deal of effort was spent over the past quarter characterizing the program coals and the forms of the trace elements in the program coals. The results obtained to date are described below.

3.2.1   Coal Size Distributions, Forms of Sulfur, and Mineralogy

The three coals distributed thus far were all pulverized by the supplier in a small pilot scale pulverizer. Samples of these coals were then size and density segregated using a sieve technique and a fluidized bed apparatus described in the last quarterly report.[1] The resulting coal particle size distributions are shown in Figure 3-1. As can be seen from this figure, all of the coals had very similar particle size distributions.
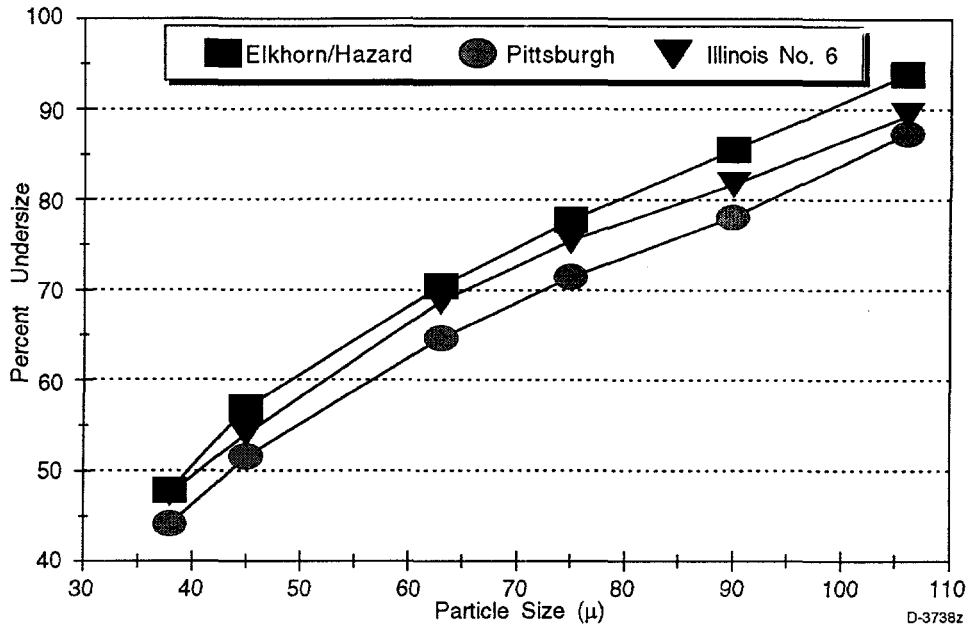
Figure 3-1. Coal particle size distributions for three bituminous coals.

The forms of sulfur analysis for all three program coals distributed to date was also repeated during the last quarter. In the last quarterly report[1] discrepancies were noted between the total sulfur measured by the commercial laboratory and that derived from the USGS analysis. A repeat analysis of the Pittsburgh coal by USGS, including an ultimate and proximate analysis, confirmed their earlier results. During the analysis of this particular coal by the commercial laboratory several errors were noted (and corrected). Therefore the USGS results are considered more reliable and will be used throughout the remainder of the program. The sulfur distribution is shown in Table 3-1.

Table 3-1. Sulfur Form Data (all data in percent on a dry basis)

	Sulfate Sulfur	Pyritic Sulfur	Organic Sulfur	Totals
Pittsburgh	0.01	0.91	1.20	2.12
Elkhorn/Hazard	0.03	0.12	0.72	0.87
Illinois No. 6	0.04	1.57	2.21	3.82

The mineralogy for these coals was measured by CCSEM and presented in the previous quarterly report.[1] As part of the microprobe analysis performed by the USGS in the last quarter to determine the forms of arsenic and nickel in these coals (see Section 3.2.2), SEM was used to determine the major minerals present in each coal. This SEM analyses indicated the presence of the major minerals kaolinite, illite, quartz, pyrite, chalcopyrite, iron oxide and minor minerals rutile (possible) and rare earth phosphates in the Elkhorn/Hazard coal. In the Pittsburgh coal, the major minerals calcite, pyrite, illite, kaolinite, quartz, barite, and iron oxides were found. The

Illinois No. 6 coal contained the major minerals pyrite, illite, kaolinite, and quartz. Differing morphologies for pyrite were observed in the program coals with the SEM; these morphologies included subhedral grains, euhedral grains, and framboids. These results are similar to the CCSEM results with the exception of the reported iron oxide for the various coals. The CCSEM reported very small (0.6 wt%) iron oxide in the Pittsburgh coal. The discrepancies may be due to the smaller sample size (i.e., number of particles counted) utilized in the SEM analysis as compared to the CCSEM.

3.2.2 *Trace Element Concentrations in Coal*

The trace element concentrations measurements for the Illinois No. 6 by NAA (MIT) were completed in the last quarter. These results are shown in Table 3-2, which also includes the previously reported data for the other two coals. As can be seen from this table, the concentration of arsenic in the Illinois No. 6 coal is lower than was found in the other coals. Selenium and chromium concentrations were within the range measured in the other two coals. Mercury, however, had a much higher concentration in the Illinois No. 6.

The trace element concentrations in the three bituminous coals were also measured by the USGS. This group utilized a series of techniques, including ICP-MS, that will also be used to characterize the residual solids and the leachate solutions in the leaching test. Therefore, the same analysis was used throughout the leaching analysis. These data, shown in Table 3-3, also provide an important validation of the NAA results. In general the trends derived from these analyses are comparable to those from NAA.

Trace element analysis was also performed using NAA during the past quarter on size and density fractions of the Pittsburgh and Illinois No. 6 generated at MIT. These data, and the data for the Elkhorn/Hazard coal presented in earlier quarterly reports, were used as a baseline for the combustion experiments at MIT. The data were also used to explore the association between specific trace elements and different coal density/size fractions. The results of these analyses are depicted in Figures 3-2 to 3-6. In these figures the ratios of concentrations are presented for several elements in each coal. A ratio greater than one suggests that the element is enriched in one fraction. Although the data presented below provide some preliminary information on the partitioning of the various elements into different size/density classifications, further work is required to correlate this partitioning information with the minerals in each size classes. For example, the apparatus used to density segregate each size fraction is simply based on height in the fluidized bed. The high density fraction is defined as the material in the bottom 1/3 of the bed, the intermediate density fraction is in middle 1/3 of the bed, and the low density fraction is in top 1/3 of the bed. With this strategy the absolute density (and minerals present in each density fraction) may be different for each coal. CCSEM is currently being performed by the team members at UKy, and will be presented in the next quarterly report.

Table 3-2. Trace Element Concentrations in Three Bituminous Coals

Element	Pittsburgh		Elkhorn/Hazard		Illinois No. 6	
	Concentration (ppm)	σ (ppm)	Concentration (ppm)	σ (ppm)	Concentration (ppm)	σ (ppm)
Na	600	60	340	20	400	30
Sc	1.8	0.1	3.9	0.4	2.2	0.1
Cr	13	4	20	5	14	1
Fe	8220	790	2970	410	13700	550
Co	2.5	0.3	6.2	0.5	3.6	0.2
Zn	17	5	18	5	70	10
As	4.1	0.9	4	1.1	2.7	0.3
Se	0.62	0.51	3.1	0.8	2.2	0.4
Br	17	2	25	3	3.7	1.0
Rb	8	0.1	5.1	1.1	13	2
Sr	160	60	120	70	ND	ND
Mo	0.85	0.18	4	1	4.9	1.1
Cd	0.06	0.013	0.31	0.07	0.15	0.15
Sb	0.26	0.03	1	0.1	0.38	0.03
Cs	0.55	0.19	0.45	0.09	0.99	0.11
Ba	110	20	130	10	52	7
La	4.5	0.1	14	1	4.7	0.3
Ce	8.8	0.3	27	4	9.3	0.5
Sm	0.78	0.05	2.5	0.2	0.9	0.08
Eu	0.2	0.06	0.37	0.12	0.19	0.02
Yb	0.38	0.06	1.4	0.2	0.032	0.021
Lu	0.063	0.005	0.24	0.02	0.0054	0.0022
Hf	0.44	0.04	1.1	0.2	0.056	0.021
Au (in ppb)	0.95	0.22	0.98	0.49	0.51	0.08
Hg	0.11	0.04	0.13	0.03	0.22	0.02
Th	1.2	0.1	4.3	0.5	0.095	0.035
U	0.31	0.15	1.9	0.8	ND	ND

Table 3-3. Chemical Analyses for the Pittsburgh, Elkhorn/Hazard and Illinois No. 6 Feed Coals

Element	Elkhorn/Hazard	Pittsburgh	Illinois No. 6	Analytical Technique
Ag	0.16	0.15	0.21	ICP-MS
As	5.12	4.75	3.09	
Au	0.8	0.73	1.03	
Bi	0.16	0.15	0.21	
Cd	0.06	0.06	0.41	
Cs	0.48	0.59	1.24	
Ga	8	3.58	3.81	
Ge	3.84	3.07	5.36	
Md	2.08	0.88	6.08	
Nb	3.2	1.46	2.06	
Pb	8.8	3.14	13.39	
Rb	6.56	7.15	15.45	
Sb	1.2	0.29	0.44	
Sn	0.8	0.73	1.03	
Te	0.16	0.15	0.21	
Tl	0.32	0.15	0.67	
U	2.16	0.41	1.75	
Be	3	0.6	1.1	ICP-AES
Co	7	2.4	3.6	
Cr	14.4	8.8	18.5	
Cu	19.2	5.3	8.2	
Li	18.4	5.4	7.8	
Mn	13.6	13.1	37.1	
Ni	12	6.6	12.4	
Sc	3.8	1.9	2.7	
Sr	136	124.1	27.8	
Th	3.5	1.2	1.5	
V	23.2	11.7	25.8	
Y	12.8	2.9	4.5	
Zn	6.2	6.1	73.1	
B	14.4	29.9	154.5	
Ba	112	116.8	43.3	
Zr	56	21.2	29.9	
Se	4.5	0.96	2.9	Hydride method
Hg	0.05	0.09	0.06	CV
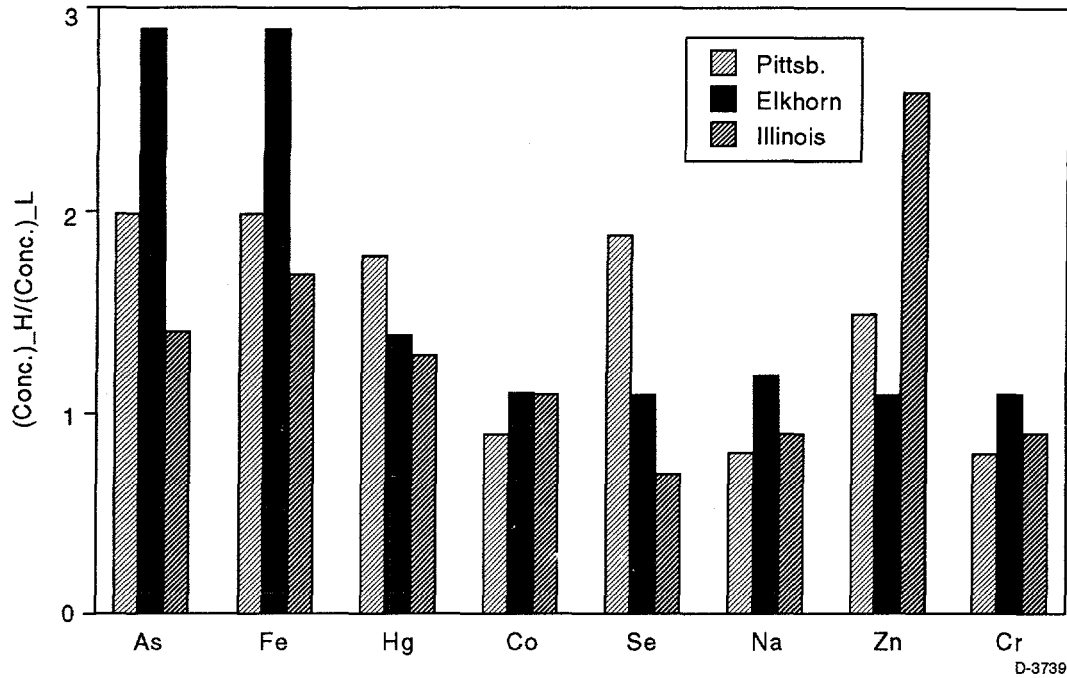
Figure 3-2. Relative trace element concentrations in two density fractions of the 45 to 65 μm cut of three bituminous coals.
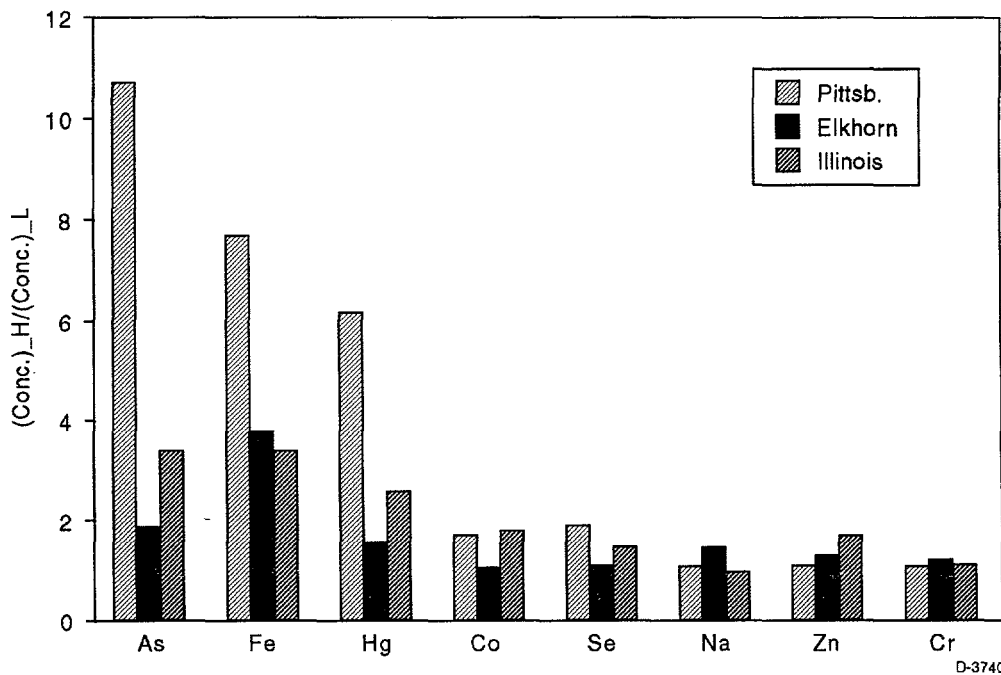
Figure 3-3. Relative trace element concentrations in two density fractions of the 90 to 106 μm cut of three bituminous coals.

3-8
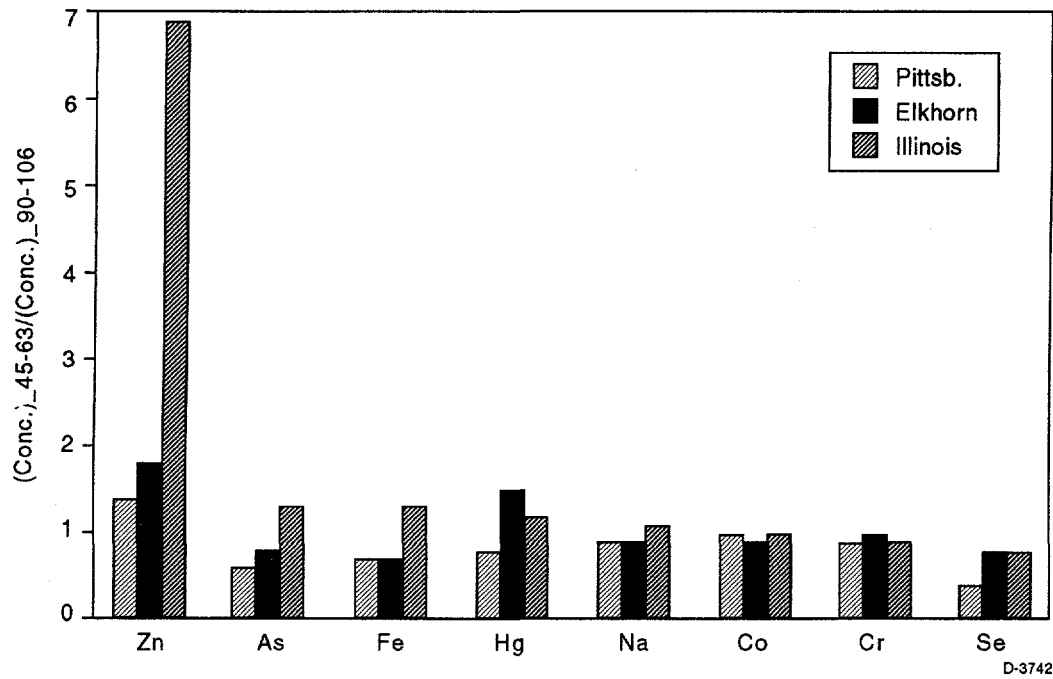
Figure 3-4. Relative trace element concentrations in two size fractions of three bituminous coals.
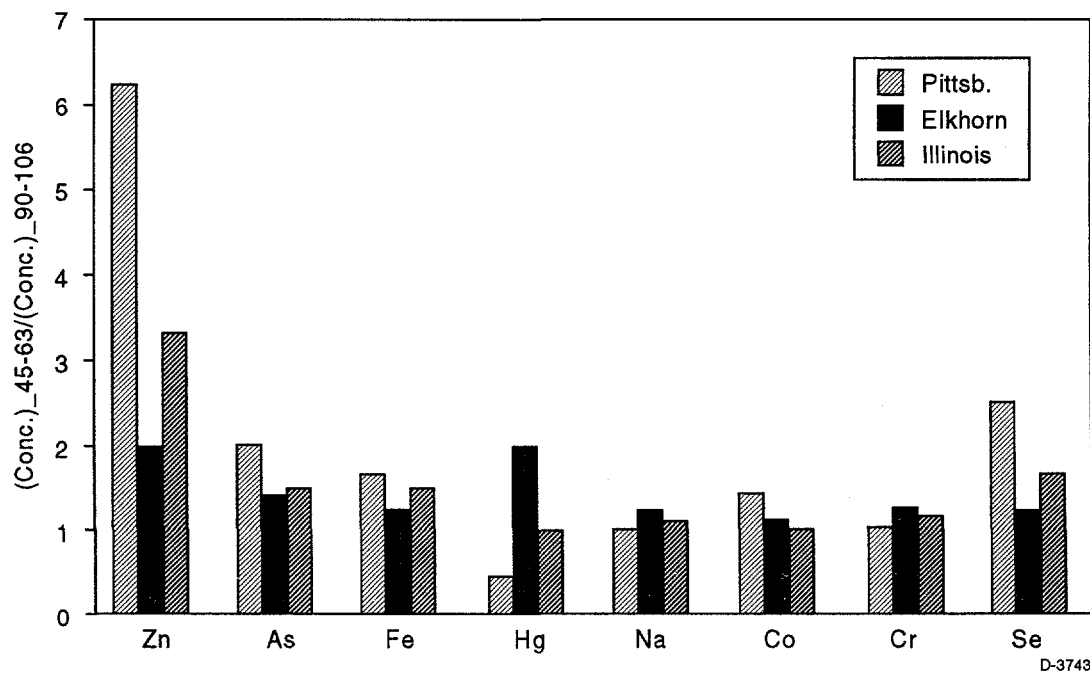
Figure 3-5. Relative trace element concentrations in the low density fraction of two size cuts of the three bituminous coals.
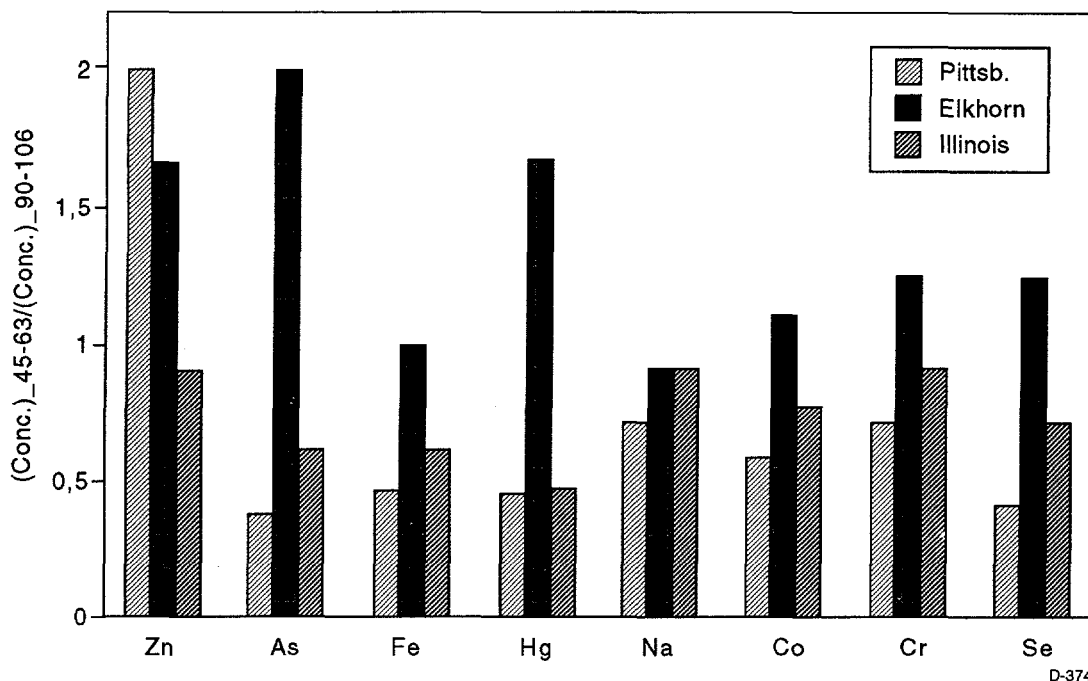
Figure 3-6. Relative trace element concentrations in the high density fraction of two size cuts of the three bituminous coals.

As shown in Figure 3-2, arsenic, zinc, mercury, and selenium are concentrated in the high density fraction (45 to 65 µm size class) of the Pittsburgh and Elkhorn/Hazard coals. For the Illinois No. 6, only zinc was enriched in the high density fraction. Arsenic and mercury were also enriched in the high density fraction for the 90 to 106 µm size range of the Pittsburgh and Elkhorn/Hazard coals. However, iron was also found to be enriched in the high density fraction in these samples (Figure 3-3).

Figure 3-4 illustrates the partitioning of the various elements between different sizes (all densities included) for a given density fraction. As shown in this figure, zinc was enriched in the smaller size fraction for all coals. Arsenic, iron, mercury, sodium, cobalt, chromium, and selenium are uniformly distributed between these two size cuts.

Figures 3-5 and 3-6 show the effect of size on the trace element concentration in a given density split. Zinc, arsenic, and selenium are enriched in the smaller sizes (low density fraction) in the Pittsburgh coal (Figure 3-5), while only zinc is enriched in this size range for the Elkhorn/Hazard coal. Generally, the elements are uniformly distributed between the two sizes in the low density cut.

For the high density cut most of the elements were found to be enriched in the larger size ranges (Figure 3-6). The only exceptions are zinc, arsenic, and mercury in the Pittsburgh coal and zinc in the Elkhorn/Hazard coal.

As mentioned above, further analysis of the minerals present in each size and density fraction is required before any correlations can be drawn between the data in Figures 3-1 through 3-5 and the forms of occurrence of the various trace elements in each size fraction. This work is currently underway and will be presented in the next quarterly report.

3.2.3   Trace Element Forms of Occurrence in Coal

As part of this program a wide array of analytical techniques and procedures are being utilized to determine the mode of occurrence of selected trace elements in coal. By utilizing complimentary analytical techniques we can determine both the physical association of the trace element (e.g., mineral or organically associated) and the chemical speciation (e.g., oxidation state) of the trace element in the coal.

As discussed in Section 3.2.1, the primary focus at the USGS has been the use of electron microprobes and selective leaching to measure trace element forms. Each of the three program coals distributed to date has been ground and cast into pellets and polished for SEM and microprobe analysis according to the procedures outlined by ASTM,[2] as modified by Pontolillo and Stanton.[3] These pellets were then examined with the SEM with an attached energy dispersive X-ray analyzer (EDXA) to (1) determine major and minor mineralogy of the samples and (2) determine variations in morphology of pyrite grains. Mineral identifications using EDXA are tentative because of its semiquantitative capabilities; however, identification of minerals can be made based on morphology and cleavage characteristics of mineral grains. Because pyrite is known to be a primary source of arsenic in coal,[4] differing pyrite morphologies were identified in the SEM analysis in order to select the grains to be analyzed quantitatively with the microprobe. Two types of SEM's were used: an ETEC Autoscan and a JEOL 840.[a] Normal operating voltage was 30 KeV, both secondary electron and back-scattered modes were used. A fully-automated, five spectrometer instrument (JEOL JXA 8800L Superprobe[a]) was used to quantitatively determine element concentrations in sulfides by the wavelength-dispersive technique. In our preliminary microprobe work with the program coals, we analyzed for the following elements: Fe, S, As, Ni and Cu. Natural and synthetic standards were used. Trace elements analyzed on the microprobe can be detected at a level of several hundred ppm; however, counting statistics at this low a level have a large uncertainty. In the probe analysis, we attempted to detect compositional differences among different pyrite morphologies. Microprobe data collected are shown in Appendix A.

The sequential leaching tests were completed in the past quarter for the three program coals received to date. The procedure used was similar to one described by Palmer et al.[5] which was modified from Finkelman et al.[6] Duplicate 5 g samples were sequentially leached with 35 ml each of 1N ammonium acetate (CH_3COONH_3), 3N hydrochloric acid (HCl), concentrated hydrofluoric acid (HF; 48%) and 2N (1:7) nitric acid (HNO_3) in 50 ml polypropylene tubes. Each tube was shaken for 18 hours on a Burrell[a] wrist action shaker. Because of the formation of gas during some of the leaching procedures it was necessary to enclose each tube in two

---

[a]   Use of tradenames and trademarks in this publication is for descriptive purposes only and does not constitute endorsement by the U.S. Geological Survey.

polyethylene bags, each closed with plastic coated wire straps that allow gas to escape but prevent the release of liquid. Approximately 0.5 g of residual solid was removed from each tube for INAA. The solutions were saved for inductively coupled argon plasma (ICP) analysis. Results of these analyses are expected in the next quarter.

The group at UKy is using XAFS spectroscopy and Mössbauer spectroscopy to complement the USGS work, and to examine the mode of occurrence of key HAPs and other elements in program coals. As discussed in the first quarterly report and shown in Figures 3-7 and 3-8, the XAFS spectra of the HAPs elements are obtained not just from the raw coal (RAW), but also from three fractions: (1) an "organic-rich" fraction (ORG) - either the fraction that floats in a 1.62 specific gravity liquid or the clean product from a Denver (froth flotation) cell; (2) a "heavy-minerals-rich" fraction (HYM) - the fraction of the refuse or tailings fraction from (1) that sinks in a 2.875 specific-gravity liquid; and (3) a "clay-rich" fraction (CLAY) - the float fraction from the 2.875 specific-gravity liquid. These fractions are then taken to the synchrotron for XAFS analysis. It should be noted that the approximate weight ratios of the different fractions separated from these coals according to this scheme are estimated to be: ORG:CLAY:HYM = >90%:5-10%:<1%, depending on ash content.

Forms of Occurrence Analysis

Sample Generation Scheme
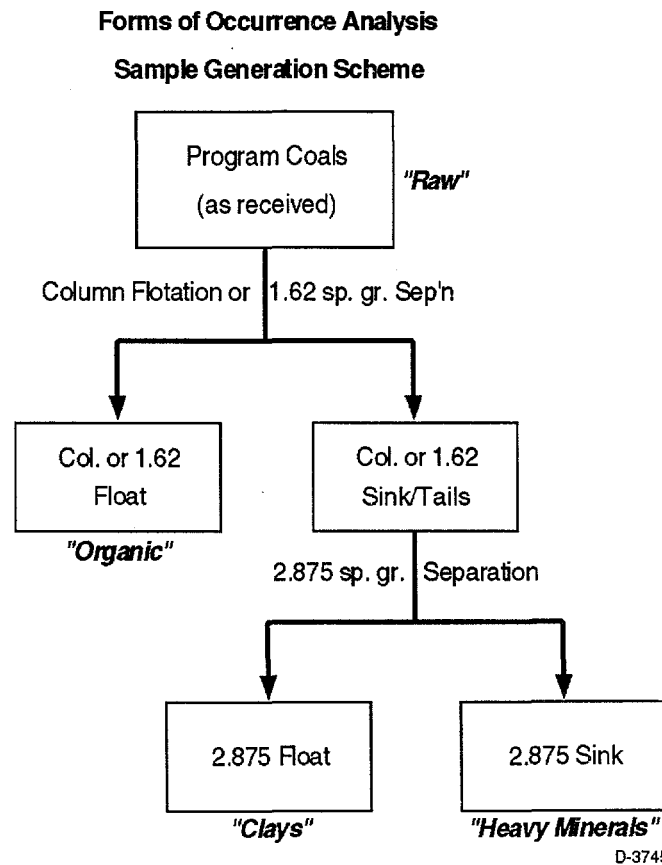
Figure 3-7. Sample separation scheme for coal fractions for XAFS analysis.

3-12
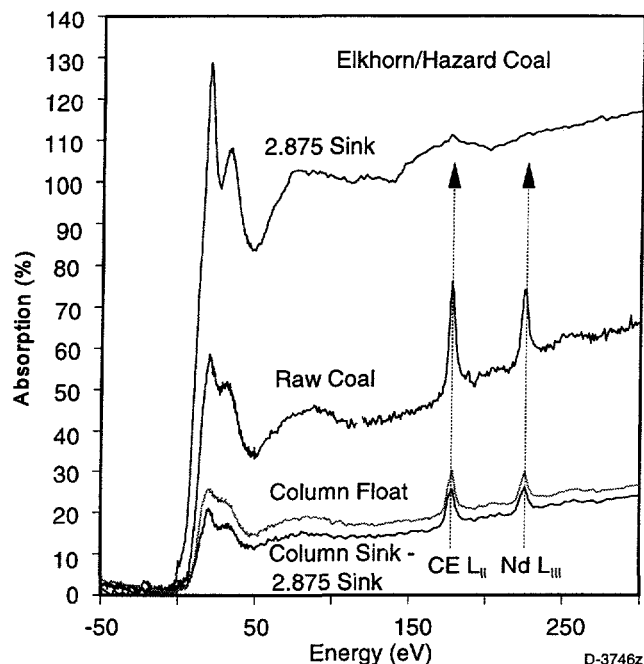
Figure 3-8. Chromium XAFS spectra for Elkhorn/Hazard coal and fractions.

As indicated in Figure 3-8 for chromium in the Elkhorn/Hazard coal, the XAFS data for the different fractions provide a wealth of qualitative and semi-quantitative information that could not be obtained from the XAFS spectrum of the coal by itself. In addition to the XANES (X-ray absorption near-edge structure - the spectral data associated with the edge) information that is used to identify the mode of occurrence of the chromium, the edge-step (defined as the difference in absorption height of the near-horizontal pre-edge and post-edge regions) is very approximately proportional to the chromium concentration in the fraction. Based on Figure 3-8, we can estimate that the chromium concentration of the "heavy-minerals" fraction is about five times that of the "organic" and "clay" fractions. Occasionally, the XAFS spectrum also supplies some gratuitous information. For example, edges for the rare-earth elements, cerium and neodymium, occur in the XAFS spectra of chromium shown in Figure 3-8. For whatever its worth, the spectral data show that these rare-earth elements are absent from the heavy minerals fraction, in contrast to chromium.

To date, microprobe data have been obtained for arsenic, nickel, and copper for selected program coals. XAFS spectral data have been obtained for S, Cl, Cr, Mn, Fe, Ni, As, Se in the Elkhorn/Hazard and Pittsburgh #8 coals, and preliminary data have been obtained for S, Cl, Cr, Fe, and As in the Illinois #6 coal. The data for the individual elements will be discussed separately in the next section in order to compare and contrast the elemental modes of occurrence for the different coals.

Arsenic

Microprobe analysis indicated that the arsenic content of pyrite grains in the Illinois No. 6 (0.01 to 0.16 ppm) and Pittsburgh (0.0 to 0.18 ppm) coals are similar, and that pyrites for these

3-13

two coals were not distinguishable based on arsenic concentrations. The arsenic concentrations also did not appear to vary according to morphology of pyrite grains. However, because framboids in these coals are small (15 micrometers in diameter or less) and difficult to polish, they were not well represented in the microprobe analysis. As concentrations (0.01 to 0.373 wt% As) in pyrite grains of the Elkhorn/Hazard coal generally exceeded those in the Pittsburgh or Illinois No. 6 coals. One grain of pyrite observed in the Elkhorn/Hazard coal contained about 2 wt% As.

Arsenic XANES spectra are shown in Figures 3-9 and 3-10 for Elkhorn/Hazard and Pittsburgh #8 fractions, respectively. All the spectra, except possibly for the HYM fractions, indicate the presence of two distinct forms of arsenic: arsenical pyrite and arsenate (AsO_4^{3-}); the arsenate is believed to be formed from the arsenical pyrite by oxidation upon exposure of the coal to the atmosphere.[7,8] Except for the spectrum of the HYM fraction, all fractions of the Elkhorn/Hazard coal show significant oxidation, with the ORG fraction exhibiting slightly more oxidation than CLAY or RAW fractions. A similar result is seen for the Pittsburgh coal, except that the overall degree of oxidation is much less. Although the peak is difficult to see in these spread-out plots in Figures 3-9 and 3-10, both As XANES spectra of the HYM fractions of the two coals show a weak peak at about 70 eV that is diagnostic for arsenical pyrite.[7,9]

Data on the relative step heights for these spectra for the Elkhorn/Hazard and Pittsburgh #8 coals are summarized in Table 3-4. These data confirm that the arsenic is significantly more concentrated in the HYM fraction than in the other fractions. However, it should be noted that the CLAY fractions also contain significant enrichments of arsenic as well. Also summarized in Table 3-5 are the percentages of arsenic found in pyritic and arsenate forms in the coal and coal fractions. These data were obtained from the XANES spectra by means of a calibrated least-squares fitting procedure.[8,20]
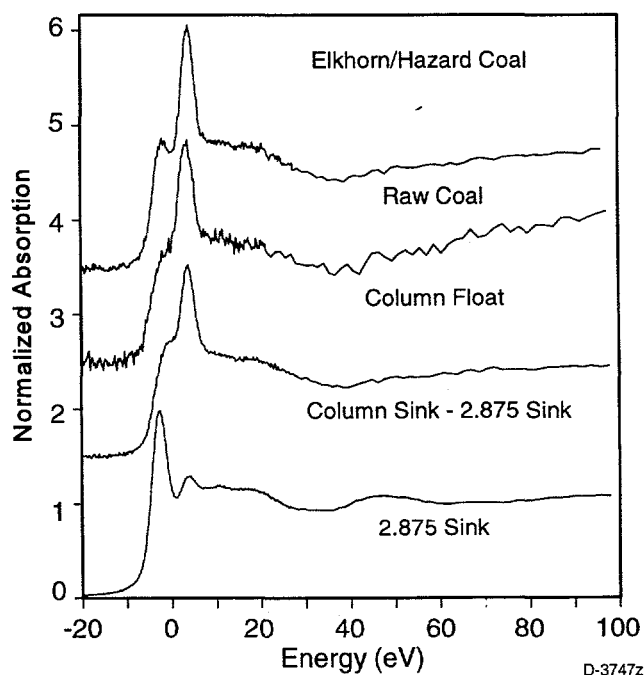
Figure 3-9. Arsenic XANES spectra for Elkhorn/Hazard coal and fractions.
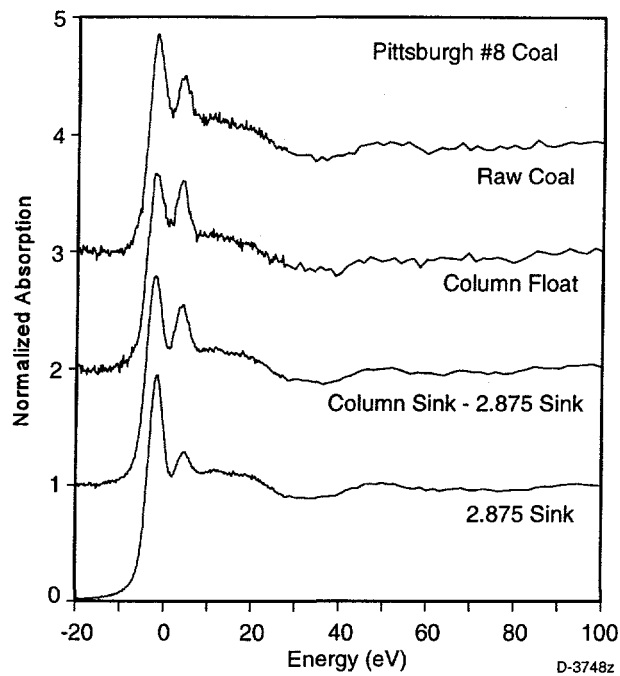
Figure 3-10. Arsenic XANES spectra for Pittsburgh #8 coal and fractions.

Table 3-4. Arsenic Forms of Occurrence Determined from As XANES

Coal Sample Fraction	Relative Step-Height	% As as Pyrite	% As as Arsenate
Elkhorn/Hazard RAW	1.0	61	39
ORG	0.6	55	45
CLAY	2.1	64	36
HYM	4.0	94	6
Pittsburgh #8 RAW	1.0	88	12
ORG	0.9	83	17
CLAY	2.8	86	14
HYM	5.0	93	7

Table 3-5. Cr Step-Heights for Different Fractions for the Three Project Coals

Fraction	Elk/Hazard	Pittsburgh #8	Illinois #6
RAW	1.0	1.0	1.0
ORG	1.0	0.8	0.7
CLAY	0.7	1.6	0.4
HYM	5.0	0.6	0.4

Perhaps the most surprising result is the almost total lack of arsenate present in the 2.875 sink fractions in contrast to the other fractions. It should be noted that even the small amounts of arsenate listed in Table 3-4 for the HYM fractions are most likely an artefact of the fitting as the As XANES spectra of a freshly crushed arsenical pyrite standard also has a similar-sized small peak located near to the arsenate peak position. A possible explanation for this observation is that there are at least two distinct forms of arsenic-containing pyrite in the sample: one is coarse, unoxidized, and segregates strongly to the 2.875 sink fraction, while the other form is fine, oxidized, and dispersed in clays or the macerals.

Chromium

Chromium XAFS data have been obtained from the fractions prepared from the Elkhorn/Hazard, Pittsburgh #8, and Illinois #6 coals. In Table 3-5, the relative step-heights are listed for the different fractions from all three coals.

The raw XAFS data shown in Figure 3-8 for chromium in Elkhorn/Hazard coal has been manipulated to give the Cr XANES spectra shown in Figure 3-11. As can be seen more clearly from this figure, the Cr XANES spectrum and the corresponding derivative of each fraction are quite different from those of the other two fractions. This implies that there are three distinct chromium forms present in Elkhorn/Hazard coal and, furthermore, each form is concentrated in a different fraction. Based on comparison with standard compounds and earlier work,[7,8] the three forms have been identified as follows: (1) a poorly crystalline Cr oxyhydroxide (CrOOH) phase associated largely with the coal macerals; (2) a form consisting of Cr in illite associated predominantly with the clay fraction; and (3) a chrome spinel of general composition, $(Fe,Mg)(Cr,Al,Fe)_2O_4$, found largely in the heavy minerals fraction.

The Cr XANES of the fractions of the Pittsburgh #8 and Illinois #6 coals (not shown) indicate that chromite is not significant in the HYM fractions (note the low step-height values listed in Table 3-5 for this fraction in contrast to that for the Elkhorn/Hazard coal) and, hence, Cr is present in these two coals only as CrOOH and as Cr/illite. However, recalling the relative approximate weights for the different fractions, it would appear that Cr is predominantly present in all three coals in the CrOOH form, with a minor amount of Cr present as Cr/illite. The chromite form in Elkhorn/Hazard coal is also quite minor in comparison to the CrOOH form.

3-16
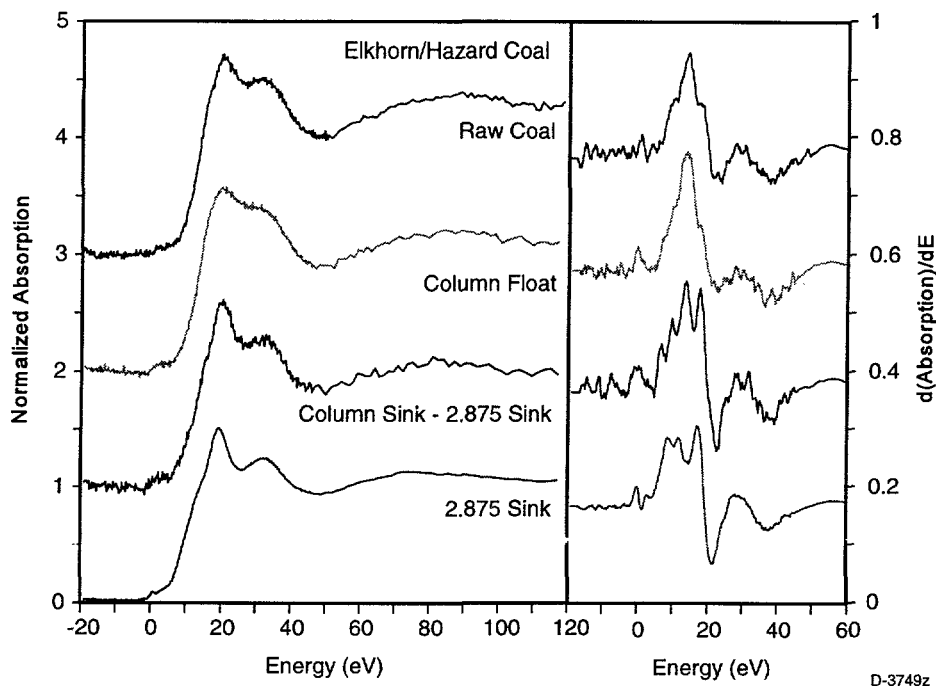
Figure 3-11. Chromium XANES spectra for Elkhorn/Hazard coal and fractions.

None of the XANES spectra measured for these three coals indicate the presence of detectable amounts of the Cr(VI) oxidation state in any fraction. Hence, it can be safely concluded that the oxidation state of chromium in these three coals is entirely Cr(III).

Chlorine

Chlorine XAFS spectra have been obtained from all three raw coals. It was felt that it would not be worthwhile to examine the fractions at the Cl edge because (1) previous work[11] has established that all of the chlorine in virtually every coal examined was associated with the coal macerals, and (2) chlorinated solvents (e.g., perchloroethylene) had been used to separate some of the fractions. The Cl XANES spectra of the coals are shown in Figure 3-12. The Cl XANES spectra of the Elkhorn/Hazard and Pittsburgh #8 coals are typical of those seen for most bituminous coals and indicate that the chlorine is present in these coals in the form of chloride anions present in the moisture associated with the coal macerals.

The Cl XANES of the Illinois #6 coal, however, is different. Although the spectrum has much in common with the other two spectra, the splitting of the main peak has been rarely observed in previous studies of chlorine in coal. We suspect that the very low chlorine content (estimated as 0.035 wt%) of this particular coal may be reflected in its unusual feature.

Selenium

Some preliminary data on Se in the program coals have been obtained. For one fraction, the HYM fraction of the Elkhorn/Hazard coal, a full 10 scans at the Se edge were accumulated.

3-17
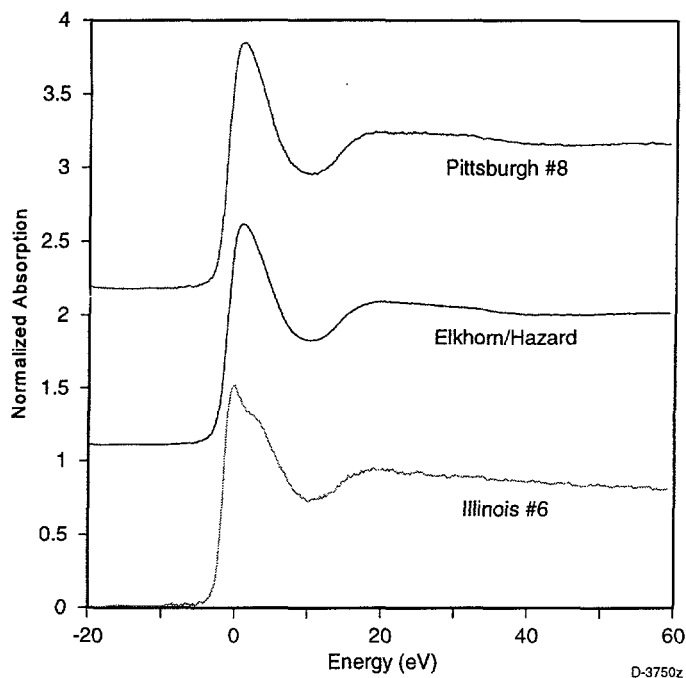
Figure 3-12. Chlorine XANES spectra for all three program coals so far received.

No other fraction has been examined in such detail, although single scans of the raw Elkhorn/Hazard and Pittsburgh #8 coals were also run for quick comparison purposes as the session at SSRL came to a close. As shown in Figure 3-13, a reasonably strong spectrum was obtained from Se in the HYM fraction of the Elkhorn/Hazard coal. Furthermore, it was readily apparent that the Se spectrum was closely similar in profile to that of As in the same fraction.

This close similarity, which extends as far out in the EXAFS region as the Se EXAFS oscillations can be seen, indicates that these elements occupy the identical site in the pyrite structure. Hence, both As and Se substitute for S in the pyrite structure in the HYM fraction of the Elkhorn/Hazard coal.

Although only a single XANES scan was made of the Se in the raw Elkhorn/Hazard coal, it was sufficiently intense and structured that it could be concluded that it arose from a quite different form to that in the HYM fraction, but that the Se concentration was of similar level. The difference in profile indicates that the coal is likely to contain other significant forms of Se than the pyritic Se. However, because pyrite is only about 0.3 wt% of the coal, Se associated with pyrite is likely to be a relatively minor form of Se in this coal.

Further work is planned on determining the Se forms in other fractions of the Elkhorn/Hazard coal and other program coals.

3-18
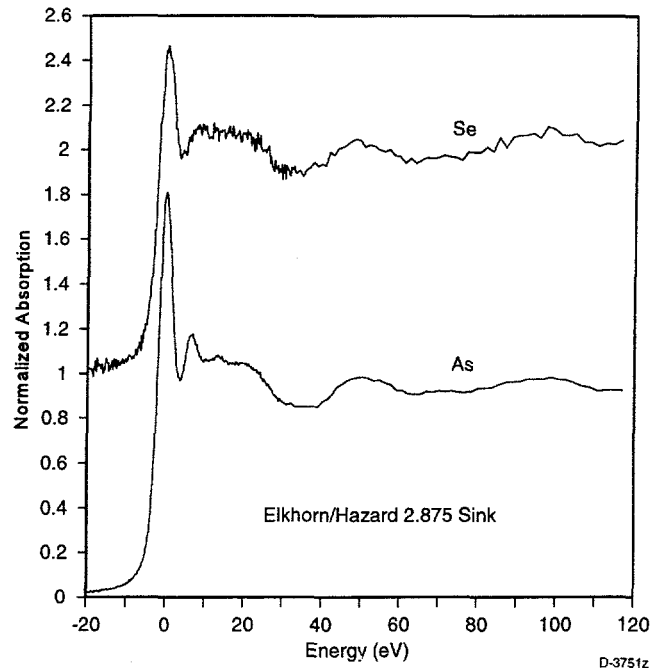
Figure 3-13. Comparison of Se XANES and As XANES spectra for the Elkhorn/Hazard HYM fraction.

Iron

Mössbauer studies of the iron mineralogy in the three program coals received to date have been completed. These data were reported in the previous Quarterly Report. In this report, we present data for all of the float/sink fractions prepared from the coals. Mössbauer investigation of iron in these coal fractions is necessary to provide additional information on the major minerals, and to correlate some of the XAFS data on trace elements with data for pyrite, a likely host mineral for many of the chalcophile elements (As, Se, Hg, Ni, etc.) of interest. Mössbauer data for the three coals and their fractions are summarized in Tables 3-6 to 3-8.

It is interesting to correlate the Mössbauer data for Fe and the XAFS data for As for the Elkhorn/Hazard coal. Based on the XAFS data in Table 3-4, this coal contains significant amounts of arsenate, an oxidized form of arsenic, in the coal and in all fractions except the HYM fraction. Further, as summarized in Table 3-6, the Mössbauer data indicate that the occurrence of jarosite, an oxidation product of pyrite, is significant in the coal and in all fractions except the HYM fraction. By both techniques, then, the HYM fraction is found not to have any significant oxidation product. In those fractions that are oxidized, the percentage of Fe as oxidation product appears to be less than the percentage of As as oxidation product. This difference would appear to indicate that it may be the arsenic-rich pyrite grains that are most susceptible to oxidation.

Figure 3-14 compares the arsenic step-height data (approximately proportional to the As content), listed in Table 3-4, with the Mössbauer determination of the wt% pyritic sulfur, listed in Tables 3-6 and 3-7, for the Elkhorn/Hazard and Pittsburgh #8 coals and fractions. Each

3-19

Table 3-6. Mössbauer Data Elkhorn/Hazard Coal

	Abs	I.S.	Q.S.	% Fe	Spyr	H0
(1) Raw Coal MK2308	Pyrite	0.31	0.61	57	0.145	
	Fe/Clay	1.13	2.61	22		
	Siderite	1.22	1.80	9		
	Jarosite	0.37	1.25	12		
(2) Column Float MK2352	Pyrite	0.31	0.61	56	0.115	
	Fe/Clay	1.14	2.59	21		
	Siderite	1.23	1.86	9		
	Jarosite	0.34	1.22	14		
(3) Column Sink/ Bromo Float MK2349	Pyrite	0.32	0.61	58	0.40	
	Fe/Clay	1.13	2.62	27		
	Jarosite	0.39	1.32	5		
(4) Bromoform Sink MK2355	Pyrite	0.31	0.60	52	12.6	---
MK2358*	Siderite	1.23	1.80	14		---
	Other	0.54	1.38	4		---
	Hematite?	0.30	-0.01	13		484
	Goethite?	0.31	-0.12	18		331

* Expanded velocity scale to include magnetic phases

Table 3-7. Mössbauer Data Pittsburgh #8 Coal

	Abs	I.S.	Q.S.	% Fe	Spyr
(1) Raw Coal MK2309	Pyrite	0.30	0.61	96.5	0.8
	Fe/Clay	1.12	2.66	1.5	
	Jarosite	0.44	1.08	2.0	
(2) Column Float MK2351	Prytie	0.29	0.61	98.0	0.7
	Fe/Clay	1.08	2.84	2.0	
(3) Column Sink/Bromo Float MK2350	Pyrite	0.30	0.61	93.0	1.60
	Fe/Clay	1.14	2.67	7.0	
(4) Bromoform Sink MK2353	Pyrite	0.29	0.61	100.0	15.6

Table 3-8. Mössbauer Data Illinois #6 Coal

	Abs	I.S.	Q.S.	% Fe	Spyr
(1) Raw Coal MK2373	Pyr/Marc	0.285	0.59	100	1.40
(2) 1.6 (PCE) Float MK2380	Pyrite Clay	0.30 1.10	0.58 2.72	97 3	0.71
(3) 1.6 Sink/2.875 Float MK2395	Pyrite	0.29	0.59	100	9.60
(4) 2.875 (Bromo) Sink MK2385	Pyrite	0.29	0.60	100	34.0
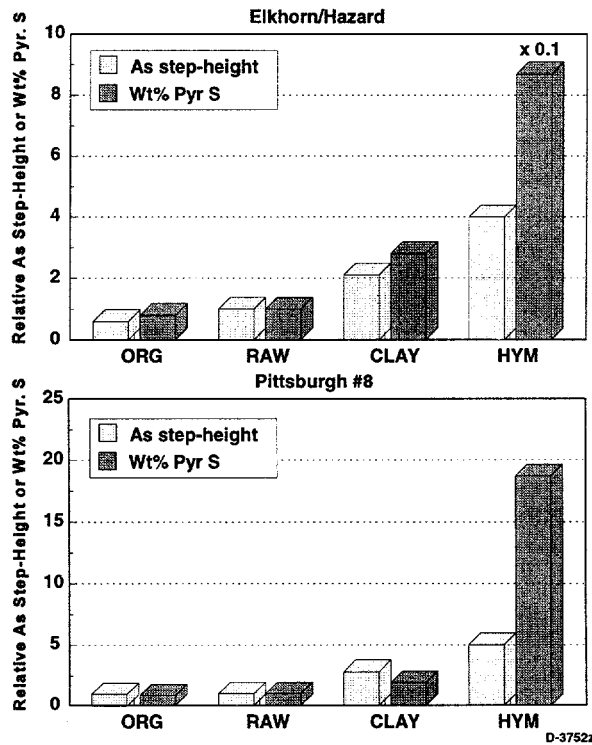
Figure 3-14. Comparison of relative arsenic concentrations (estimated from XAFS step-height) and pyrite concentrations (from Mössbauer data, Tables 3-6 and 3-7) for the Elkhorn/Hazard and Pittsburgh #8 coals and fractions.

determination is normalized to unity for the raw coal to facilitate comparison. As can be seen, the relative arsenic and pyritic sulfur trends are comparable in the ORG, RAW, and CLAY fractions, but that the HYM fraction is clearly relatively deficient in arsenic, especially for the Elkhorn/Hazard coal.

We can rationalize these observations by postulating that there are two distinct types of pyrite in these two coals. One type would have a low or perhaps even a negligible arsenic content, be less susceptible to oxidation, exhibit a coarse particle size, and report predominantly to the HYM fraction. The other type would be significantly richer in arsenic, be much more susceptible to oxidation, have a small particle size, and not be well separated by the float/sink processing. USGS did not see the aforementioned distinction between pyrite grains. However, as discussed on pages 3 through 13, their method has difficulty measuring arsenic in small (< 15 µm) pyrite grains.

Nickel

Microprobe analysis indicated that nickel is generally negligible in pyrite of all of the program coals. Exceptions include two framboids in the Illinois No. 6 coal having concentrations of 0.26 wt.% and 0.095% Ni (analysis 8.1 - pellet b).

Single scan XAFS data were taken at the Ni K-edge of the HYM fractions for the Elkhorn/Hazard and Pittsburgh #8 coals. The intent here was to see if there was a concentration enhancement of nickel that would indicate that nickel was strongly associated with pyrite in either coal. However, only very weak signals were obtained, supporting the results from the microproble analysis; Ni in pyrite was not significant.

Manganese

XAFS data have been obtained at the manganese K-edge the Elkhorn/Hazard and Pittsburgh #8 coal samples (Figure 3-15). The different forms of manganese contributing to these spectra have not yet been determined. The spectra are not readily attributed to any standard that we have examined;[9] however, it should be noted that our database of Mn standard compounds and minerals is relatively limited. Possibly, the Pittsburgh #8 can be attributed in part to Mn in carbonate. If scheduling of beam-time permits, we may examine the separated fractions of these coals in order to resolve this issue.
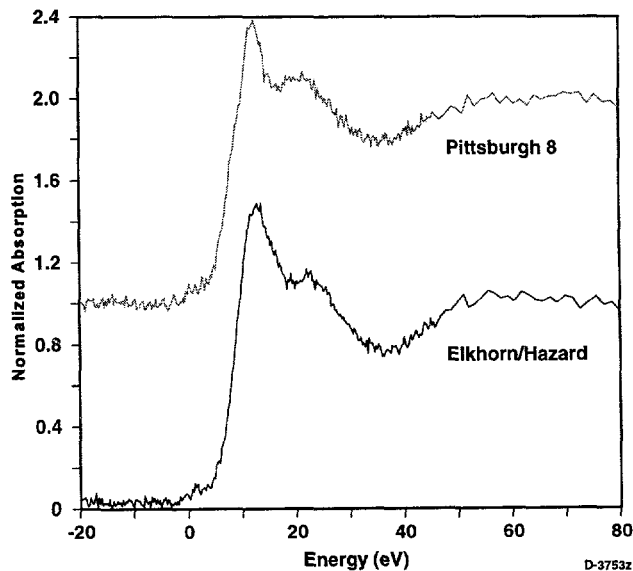

Figure 3-15. Manganese XANES spectra for the Elkhorn/Hazard and Pittsburgh #8 coals.

3-22

Sulfur

XAFS spectra have also been obtained for sulfur in the three program coal samples. These spectra have yet to be analyzed and a discussion of the results will be deferred to a later report.

3.2.4 High Mercury Coal from Washington State

One element for which we have virtually no XAFS data is mercury. To rectify this situation, we have started to obtain XAFS data on mercury standard compounds and minerals, and also on high-mercury coals. We have recently completed an XAFS investigation of a coal that contains 8.8 ppm of mercury and we acknowledge the cooperation of M. Brownfield and R. Finkelman, U.S. Geological Survey, who were able to supply us with this particular sample from Washington State. As was done for the program coals, ORG, CLAY, and HYM fractions were prepared for XAFS analysis from the raw coal using float/sink procedures. The coal and related fractions were examined at the Stanford Synchrotron Radiation Laboratory at the L_{III} edge of mercury, which occurs at about 12,284 eV.

The Hg XANES spectra of the raw coal and of a number of mercury standard compounds measured in transmission are shown in Figure 3-16. As is common with most mercury compounds, the fine structure associated with the absorption edge is rather weak and to accentuate the differences, the first derivatives of the spectra are also shown. None of the spectra of the standards is an exact match for the spectrum of the coal. The closest standard would appear to be the red form of HgS; however, some of the fine structure present in the spectrum of HgS (red) is definitely not present in the coal spectrum. The spectra of the coal and the three fractions are compared in Figure 3-17. As can be seen from this figure, the spectra of all four samples are virtually the same, implying that mercury exists predominantly in a single form in this coal.

Mössbauer studies of the high-mercury coal and fractions have also been obtained for comparison with the Hg XAFS data. These results are summarized in Table 3-9. It would appear that the iron is found exclusively in this sample of coal in the form of pyrite and its oxidation products. Both ferrous (szomolnokite, $FeSO_4.H_2O$) and ferric (jarosite) sulfates are present in minor amounts (<10% of the total iron) in all samples. Figure 3-18 shows a comparison of the Hg edge-step, a rough measure of the Hg concentration, and the wt% pyritic sulfur in the coal and fractions. Although both the Hg and pyrite concentrations vary in the same order in the suite of samples, the change in pyrite concentration is much larger, by about a factor of 5, than the change in Hg concentration. One interpretation of this trend is that the mercury is no more than 20% associated with the pyrite. A second alternative, as was suggested above for arsenic in the program coals, is that there may be two distinct generations of pyrite in the coal: one that does not contain any mercury, and one that is significantly enriched in Hg. Of these two generations, the mercury-bearing generation is only poorly separated by the float/sink processing, whereas the mercury-free generation is efficiently separated by the same processes. Thirdly, of course, there may be no correlation between mercury and pyrite at all.
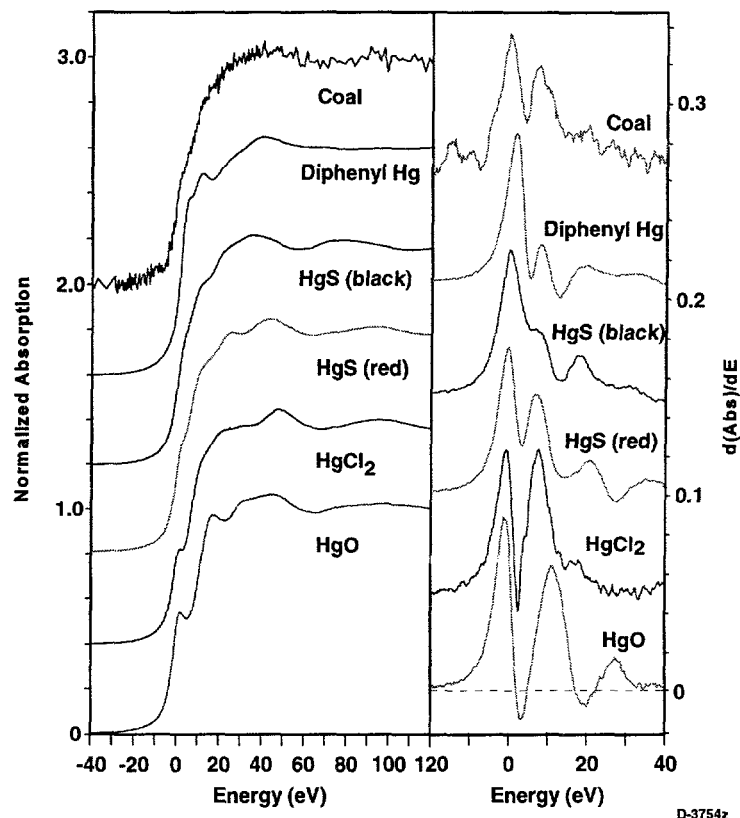
Figure 3-16. Comparison of the mercury L_{III} XANES spectra and their 1st derivative for a high-mercury coal from WA and for various mercury standards.
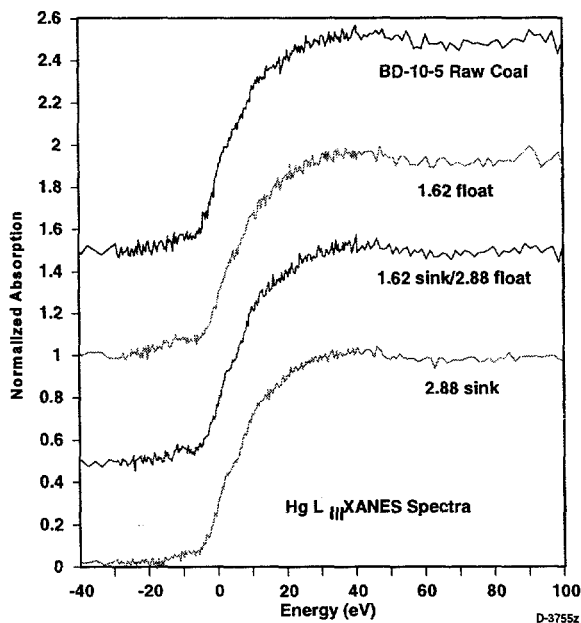
Figure 3-17. Mercury L_{III} XANES spectra for high-mercury coal from WA and fractions.

Table 3-9. Mössbauer Data John Henry Mine No. 1 Coal
(Black Diamond Mining Area, near Seattle, WA)

	Abs	I.S.	Q.S.	% Fe	Spyr
(1) Sample BD-10-5 As Rec'd Coal MK2319 MK2360	Pyrite Szomol. Jarosite	0.30 1.26 0.36	0.60 2.71 1.09	83 9 8	1.95
(2) BD-10-5 1.6 (PCE) Float MK2361	Pyrite Szomol. Jarosite	0.29 1.27 0.34	0.61 2.71 1.15	85 9 6	1.47
(3) Bd-10-5 1.6 Sink/2.875 Float MK2389	Pyrite Szomol. Jarosite	0.29 1.25 0.38	0.61 2.77 1.05	86 9 5	6.65
(4) BD-10-5 2.875 (Bromo) Sink MK2386	Pyrite Szomol. Melant.	0.31 1.26 1.25	0.62 2.70 3.20	91 4 5	22.0

Sample BD-10-5	Wt% Pyritic Sulfur (from Mössbauer)	Mercury (XANES Step-height)
1.6 Float	1.47	0.93
Raw Coal	1.95	1.00
1.6 Sink, 2.88 Flt	6.65	1.43
2.88 Sink	22.00	2.59

D-3756z

Figure 3-18. Comparison of relative mercury concentration (estimated from XAFS step-height)
and pyrite concentration (from Mössbauer data, Table 3-9) for high-mercury coal
and fractions.

3-25

In addition to the high mercury coals, R.B. Finkelman (U.S. Geological Society) has also sent us samples that are extremely enriched in selenium and arsenic. Results for these samples will be presented in subsequent reports.

3.3   Combustion Zone Transformations (MIT, PSI)

In order to better understand trace element partitioning between vapor, supermicron particles, and submicron particles it is important to understand the mechanisms that govern trace element vaporization and reaction in the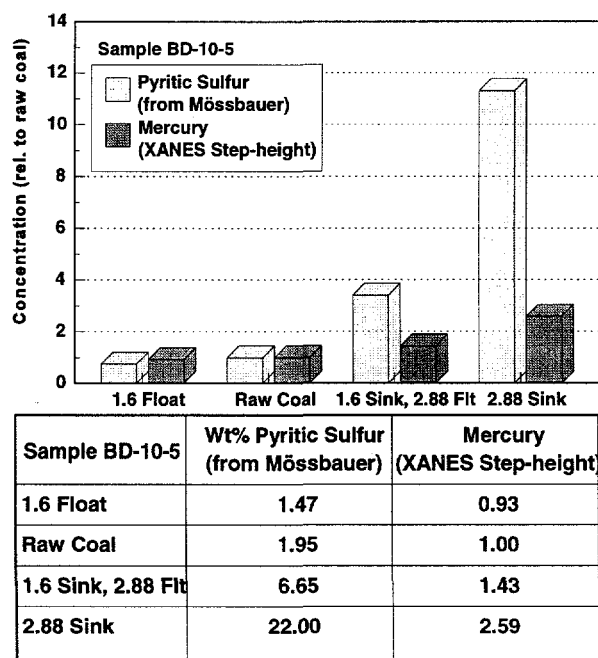 combustion zone. It is in this high temperature environment that volatile trace elements enter the vapor phase. In some cases the vapor phase metals react with other minerals present in the flame zone -- leading to partitioning of these metals to the condensed phase.

In order to fully understand the relative importance of vaporization and vapor-mineral interactions, combustion experiments are being carried out on two different combustion scales. The MIT drop tube is used to explore vaporization at high temperatures. In this apparatus the coals are burned under extremely dilute conditions (e.g., single particle studies) and mineral-vapor interactions are minimized. This effect is due to the fact that the vaporized metals are carried away from the burning coal particle (thus preventing the element from reacting with the ash from that particle). In the PSI EFR, which uses a coal number density consistent with pc-boilers, vaporized metal can react with neighboring ash/mineral particles. Thus, a comparison of these experiments yields the *net* vaporization in the combustion zone. By combining the data from these two facilities, we can decouple the vaporization and vapor-mineral reaction mechanisms and gain a better understanding of these fundamental mechanisms -- allowing us to predict vaporization and reaction with different coals and coal blends.

During the past quarter, size and size and density segregated coal samples were burned in the MIT drop-tube furnace at an oxygen concentration of 20% and a furnace temperature of 1700 K. During these experiments, the ash was segregated into two size fractions, greater than and less than 1 μm. Trace element analysis was performed on these samples and is presented for each individual element later in this section.

Also during this time period EFR experiments were completed with Elkhorn/Hazard and Pittsburgh coals. For these two experiments, the stoichiometric ratio varied from 1.0 for the Pittsburgh coal to 0.9 for the Elkhorn/Hazard coal. The furnace setpoint was 1773 K for both experiments. Ash samples were collected with both a total filter and the low pressure impactor. These experiments were originally designed as the baseline experiments for these coals (stoichiometric ratio of 1.2). However, when extremely high carbon contents were found in the ash, approximately 32 and 44% for the Pittsburgh and the Elkhorn/Hazard coals, respectively, the entire reactor system was checked for leaks. Inspection of the furnace lead to one of the mass flowmeters for the air input into the reactor, which was calibrated to a flow lower than the reading -- yielding a much lower stoichiometric ratio than expected. As these data are still very important to explore partitioning under fuel lean conditions, they will be discussed later in this section. Baseline experiments with these coals are currently underway and are expected to be completed during the next quarter.

The particle size distribution of the ash collected from the PSI EFR is shown in Figure 3-19. As can be seen from this figure, the majority of the ash is greater than 7.9 μm. This is likely due to the high residual carbon content of these ashes. The unburned carbon is likely larger than this size. The differential size distribution is shown in Figure 3-20. Also included in this figure is data from an earlier DOE sponsored program.[11] The coal denoted Pitt-1 is the sample of the Pittsburgh coal used in the earlier program, Pitt-2 denotes the sample used in the current program. Both samples came from the same mine. The coal denoted B-Thund is a PRB coal from the Wyodak-Anderson seam. The data in this plot suggest that there was much more vaporization from the earlier Pittsburgh coal and the Wyodak-Anderson coal (burned under stoichiometric ratio of 1.3) -- denoted by the larger peak size in the 0.1μm size range. This difference may be due to changes in the coal, although the analyses of the two Pittsburgh coals are similar, or may be due to the more lower stoichiometric ratio used in the current program. The baseline experiments currently underway will yield more information on this discrepancy in the ash vaporization between the two coals.

The data in Figure 3-21 show that only antimony and arsenic vaporized significantly in the EFR experiments. The top and bottom lines are the total percent vaporized for the Elkhorn/Hazard and Pittsburgh coals respectively.
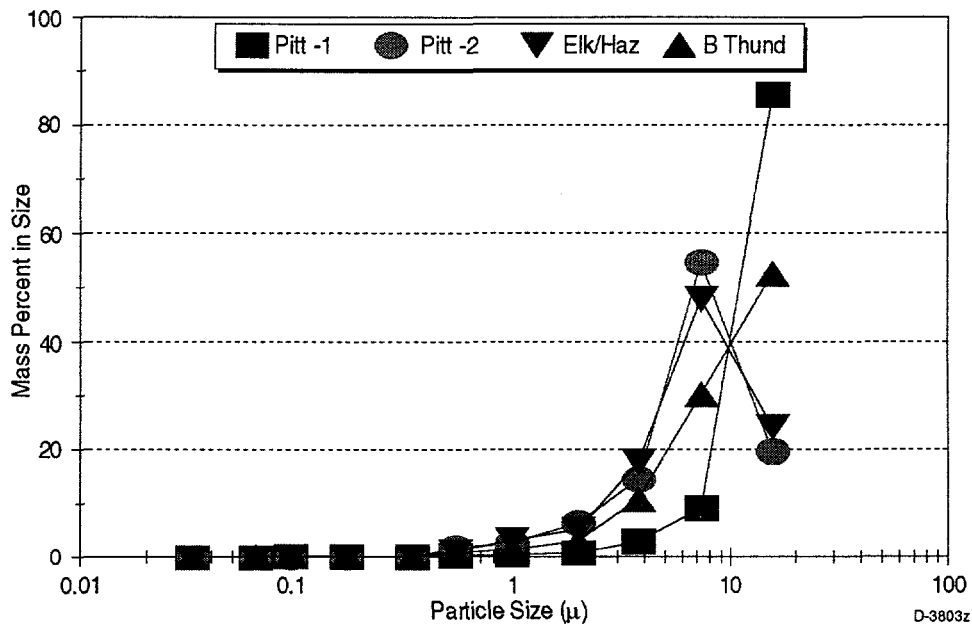

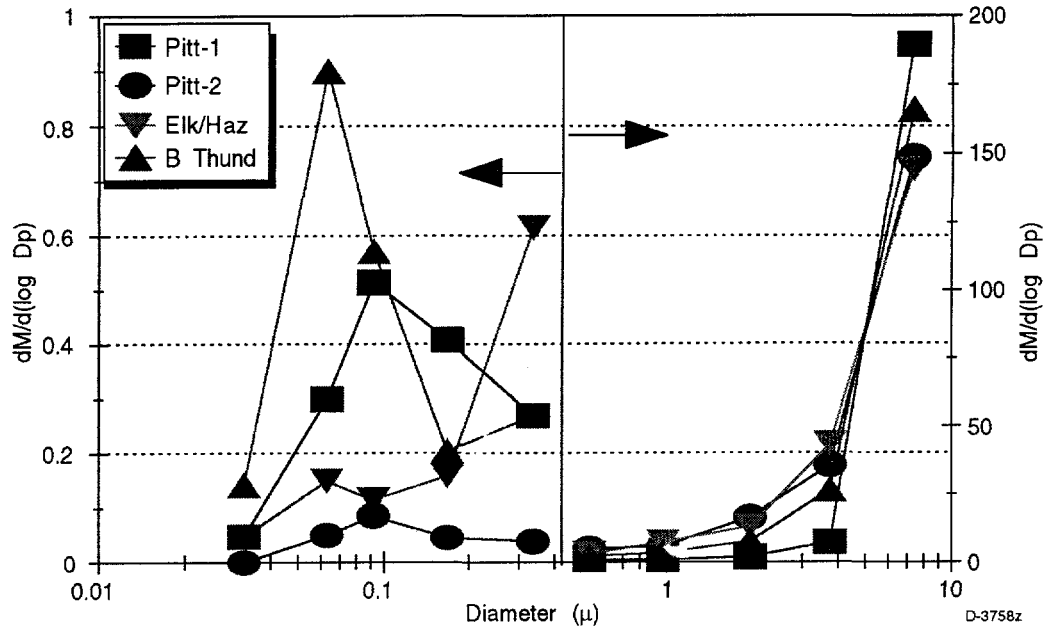Figure 3-19. Ash particle size distribution from EFR experiments.

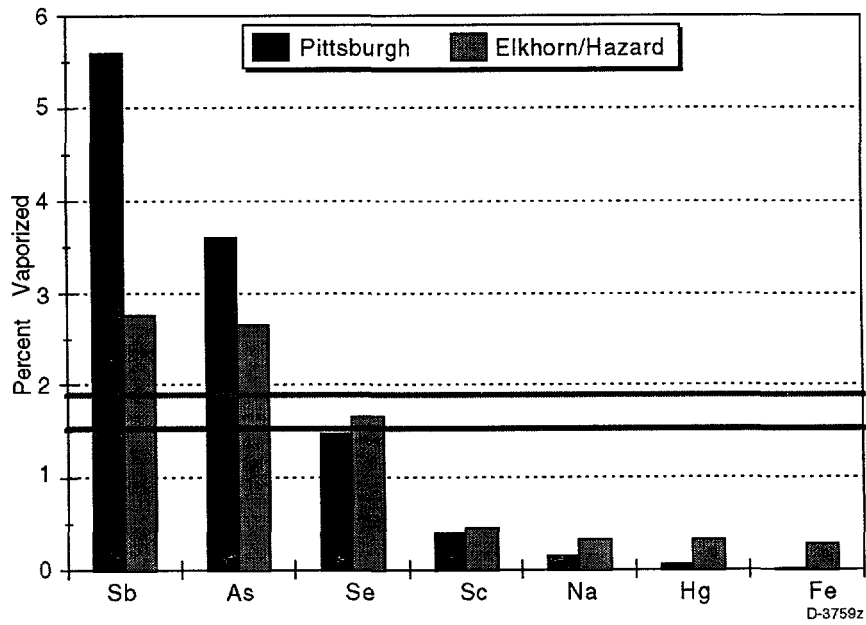Figure 3-20. Differential mass distribution from EFR experiments.

Figure 3-21. Fractional vaporization from EFR experiments (SR ~ 0.9 to 1.0).

Figures 3-22 through 3-27 illustrate another important point about trace element partitioning in the combustion zone. If the mass of a trace element correlates with the total ash mass at the exit of the combustion zone, then removal of that particular element in the air pollution control device (APCD) is simply the ash capture efficiency. However, if the ash mass does not correlate with the trace element mass (e.g., if the trace element is enriched in the small sizes) then removal of the element in the APCD may be much more difficult. To explore how the element mass correlates with the total mass, these masses are plotted in Figures 3-22 through 3-27. As shown in Figure 3-22, those elements that vaporize, and are enriched in the fine sizes, are typically above the 45 deg line for the smaller sizes and below this line for the larger sizes. The 45 deg line denotes a 1 to 1 correlation between the ash mass and the elemental mass. For example, in Figure 3-22 iron and scandium follow the 45 deg line, indicating a good correlation between the mass of these elements and the total ash mass. Arsenic, however, does not follow this trend and is enriched in the small sizes (making it more difficult to remove in an APCD). As can be seen from the following figures, antimony, arsenic, and selenium were the only elements that did not correlate with the ash distribution. Surprisingly the mercury was found to correlate well with the total ash distribution, indicating mercury capture by the residual carbon. Each element is discussed in more detail below, including the vaporization data obtained from the MIT droptube.

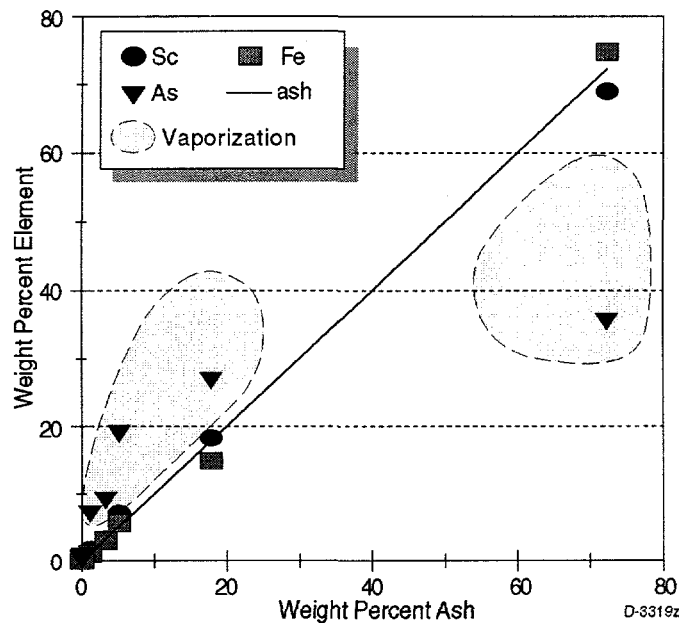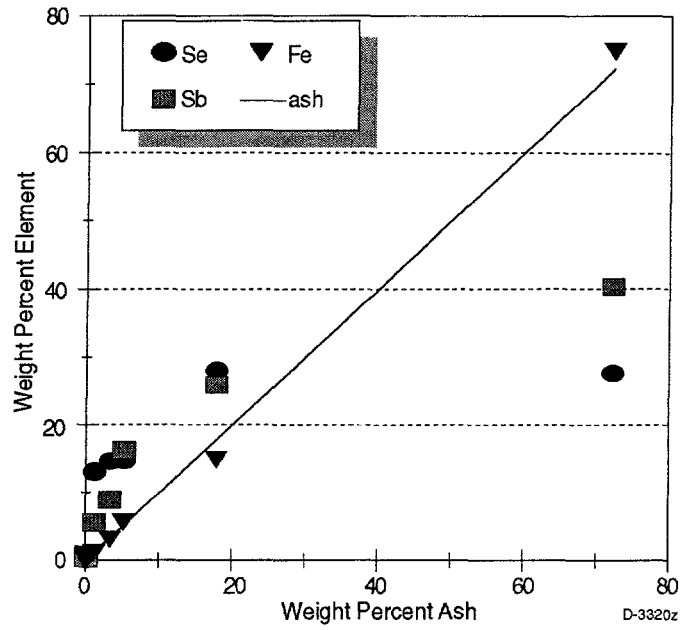Figure 3-22. Elemental and ash distribution (Sc, As, Fe) - Elkorn/Hazard (EFR: SR = 0.9).

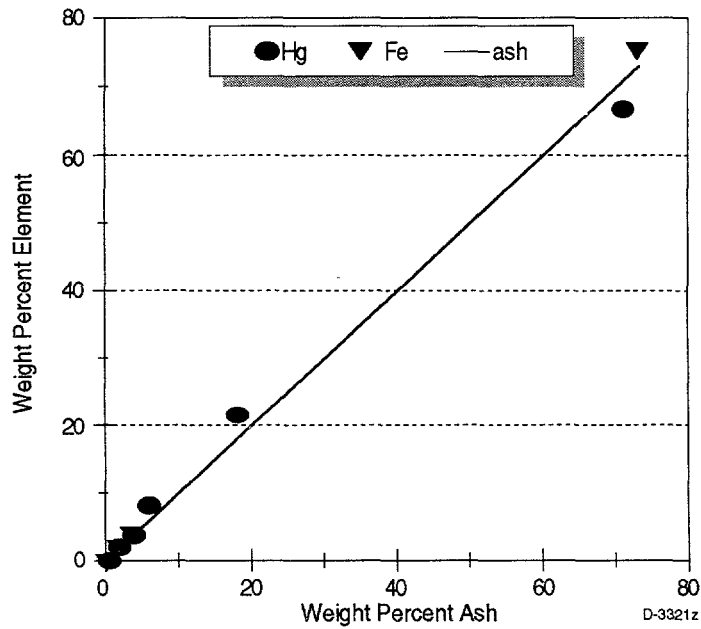Figure 3-23. Elemental and ash distribution (Se, Sb, Fe) - Elkorn/Hazard (EFR: SR = 0.9).

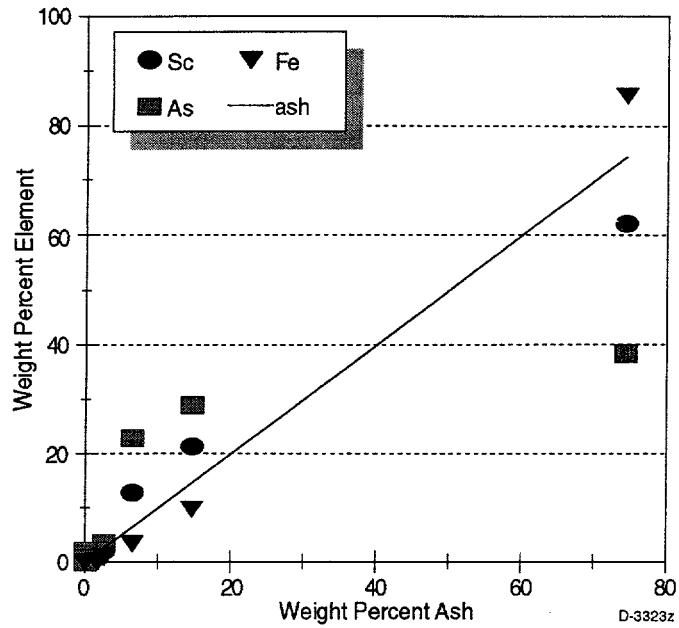Figure 3-24. Elemental and ash distribution (Hg, Fe) - Elkorn/Hazard (EFR: SR = 0.9).

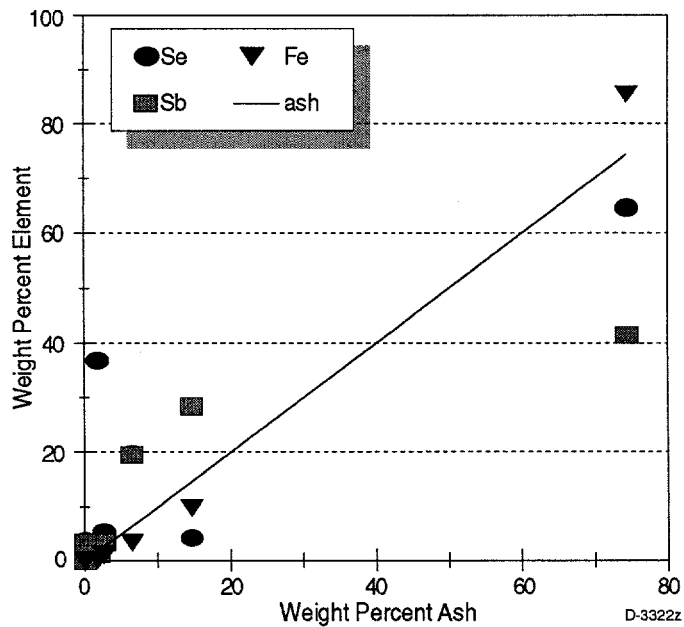Figure 3-25. Elemental and ash distribution (Sc, As, Fe) - Pittsburgh (SR = 1.0).

Figure 3-26. Elemental and ash distribution (Se, Sb, Fe) - Pittsburgh (SR = 1.0).
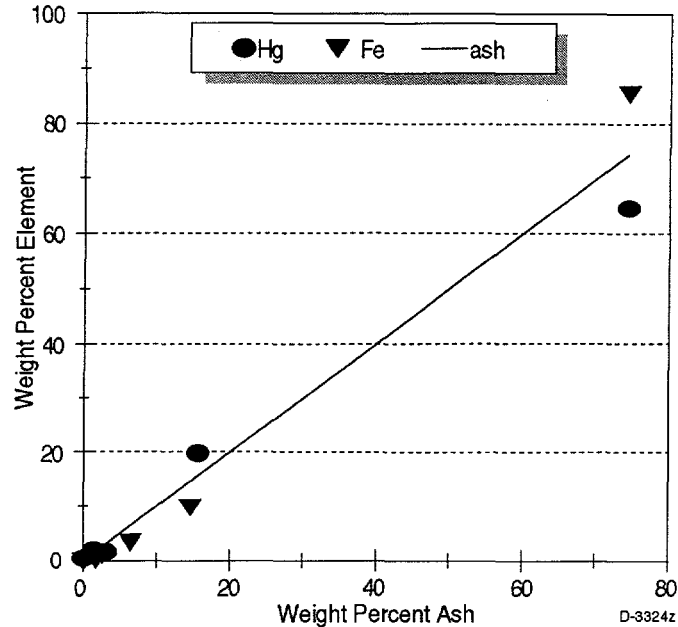
Figure 3-27. Elemental and ash distribution (Hg, Fe) - Pittsburgh (EFR: SR = 1.0).

Antimony

As shown in Figures 3-23, 3-26, 3-28, and 3-29, both the EFR experiments (PSI) and the droptube experiments (MIT) showed strong evidence of antimony vaporization. Figures 3-28 and 3-29 demonstrate that more antimony vaporized from the high density fraction of the smaller particles (45 to 63 µm) for all three coals. However, only the Illinois No. 6 showed this trend for the larger size range. Without the CCSEM data for the various density cuts it is difficult to attribute this difference in vaporization behavior to any elemental form in the coal. Earlier work with the Pittsburgh coal[11] suggested that antimony was found in both the pyrite and organically bound phases. Therfore it is likely that antimony vaporized from these two reactive matrices. This earlier work also indicated that once antimony reached the vapor phase, a substantal portion reacted with the minerals present in the coal, resulting in a large fraction this element being associated with the larger size particles. This hypothesis is supported by the large difference in the vaporization measured in the MIT drop tube furnace (Figures 3-28 and 3-29) which represents the total vaporization, and the *net* vaporization measured in the EFR (Figure 3-21). However, further work is required to clarify these results.

Arsenic

As shown in Figures 3-30 and 3-31, arsenic vaporization was much higher in the high density fraction than in the low density fraction in both size fractions for all coals. Although at first glance this result may be attributed to the pyrite-arsenic association shown earlier in this section, the fractional vaporization is a measure of how much arsenic *in that size/density* fraction vaporizes. As the coal characterization work suggested that most of the arsenic was associated with pyrite, it is likely that the arsenic in the low density fraction is found in small pyrite inclusions.

3-32
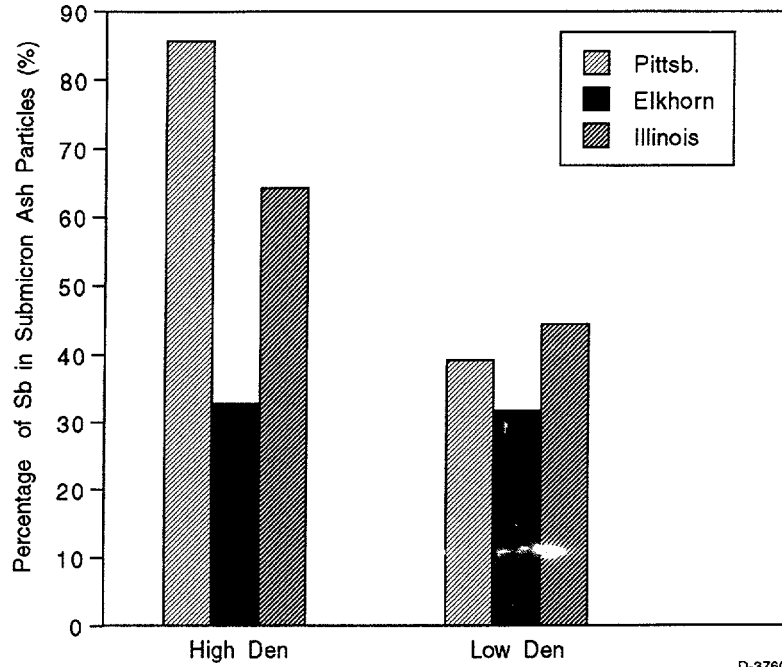
Figure 3-28. Antimony vaporization from 45 to 63 µm particles (MIT drop tube furnace).
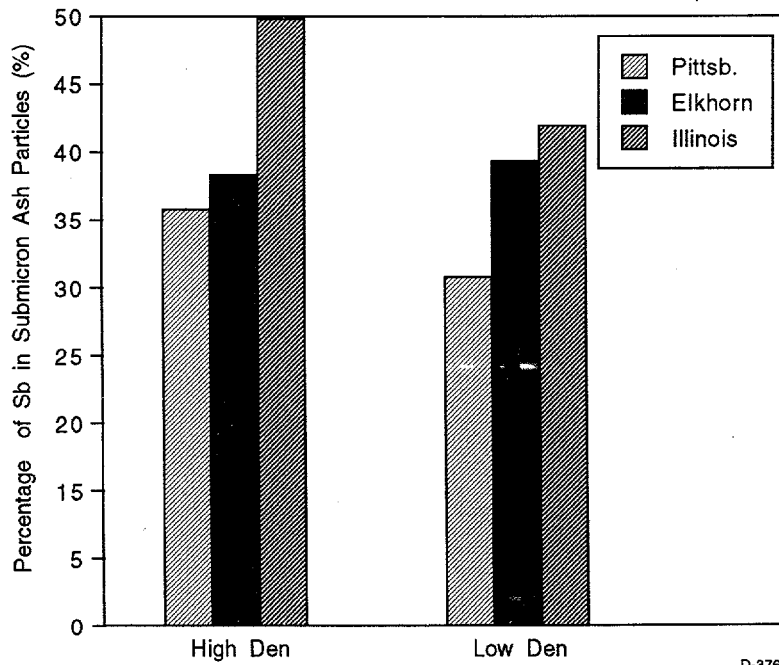
Figure 3-29. Antimony vaporization from 90 to 106 µm particles (MIT drop tube furnace).
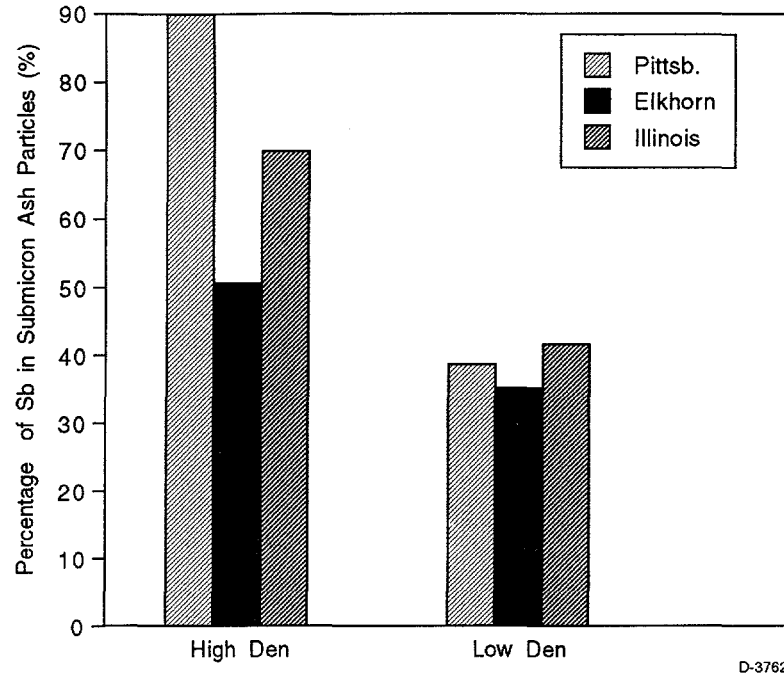
Figure 3-30. Arsenic vaporization from 45 to 63 µm particles (MIT drop tube furnace).
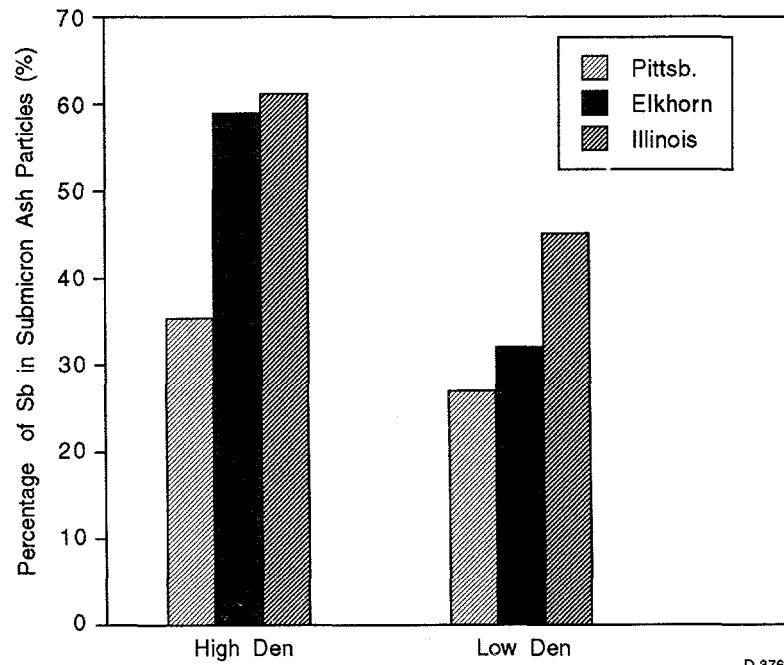
Figure 3-31. Arsenic vaporization from 90 to 106 µm particles (MIT drop tube furnace).

One possible explanation for the discrepancy is that vaporization from the pyrite depends strongly on pyrite oxidation. Sulfur oxidizes and leaves the particle during the burnout process, forming an Fe-O-S melt. As arsenic is substituted for iron in pyrite, it is possible that arsenic vaporization occurs by a similar mechanism. Inherent pyrite-derived melt phases can be captured into the glassy phase before complete oxidation of the pyrite.[12] Any unvaporized pyrite will also be captured in the glassy phase, thus reducing the arsenic vaporization from the whole coal as shown in Figure 3-21, and the arsenic vaporization from the low density fraction (Figures 3-30 and 3-31). Therefore, more arsenic can vaporize from extraneous pyrite, which oxidizes without interference from other mineral species, than from inherent pyrite. This hypothesis is further supported by the low pressure impactor data shown in Figure 3-32. In the earlier work with the Pittsburgh coal[11] the coal was burned at a stoichiometric ratio of 1.3, compared to 1.0 for the data presented in Figure 3-32 (Pitt-2). The higher stoichiometric ratio leads to a higher fractional pyrite oxidation for the earlier work (Pitt-1 in Figure 3-32), leading to higher vaporization. The stoichiometric ratio of 1.0 would result in more pyrite remaining in either a glass or an unoxidized state,[12] yielding lower observed arsenic vaporization. Both of these trends are shown in Figure 3-32, as noted by the large difference in magnitude of the 0.1 µm peak. Further work is required to fully validate this hypothesis.
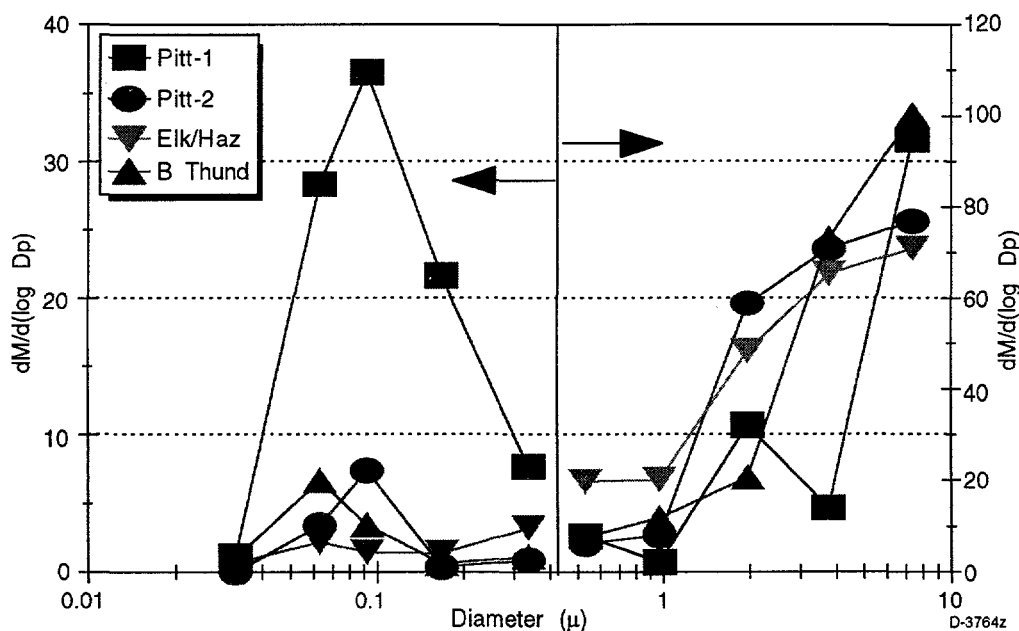
Figure 3-32. Differental arsenic mass distribution from EFR experiments.

Selenium

Figure 3-33 shows the differential mass distribution of selenium measured in the EFR. This plot shows that the lower stoichiometric ratio may have caused a decrease in the observed selenium vaporization. However, more work is required to support this conclusion.
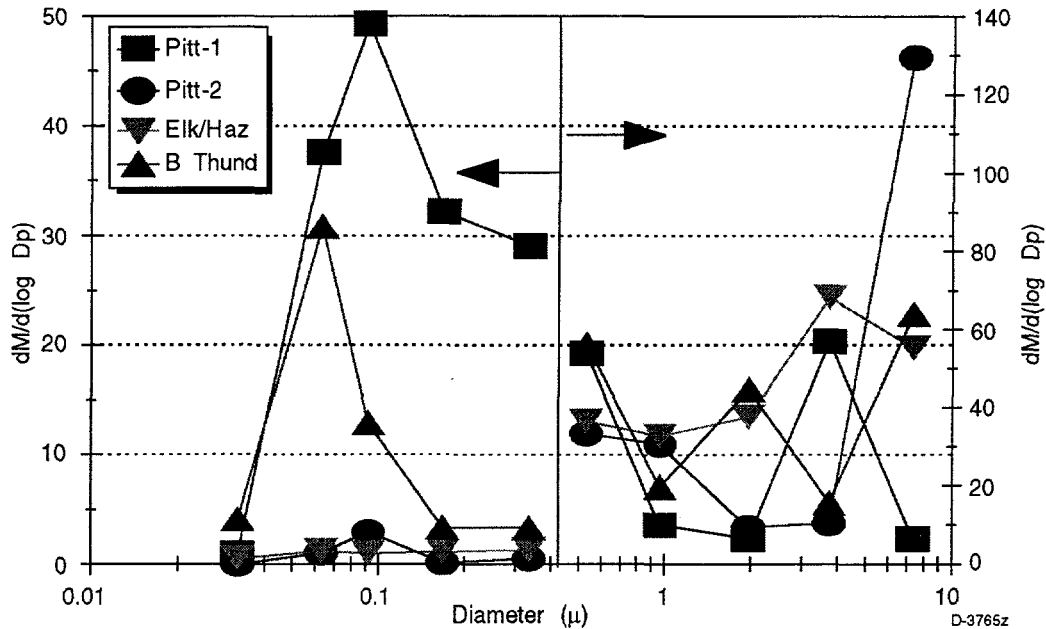
Figure 3-33. Differential selenium mass distribution from EFR experiments.

Zinc

As shown in Figures 3-34 and 3-35, zinc vaporization from the various size and density fractions was highly variable. The Pittsburgh and Elkorn/Hazard higher vaporization in the high density fraction of the 45 to 63 μm size cut. In the larger size range, more zinc vaporized from the high density cut for the Pittsburgh coal. The opposite trend was true for the Illinois No. 6 coal.

Iron

Figures 3-36 and 3-37 show that relatively little iron vaporized in the MIT drop tube furnace. This is consistent with the results from EFR (Figure 3-21).

Mercury

Figures 3-38 and 3-39 illustrate the amount of mercury found in the submicron ash from the MIT drop tube furnace. The percentage of Hg in the submicron ash is always higher for the low density cut. However, as with the EFR data (Figures 3-24 and 3-27), it is likely that the mercury in the ash samples was adsorbed onto residual carbon, and a significant amount of mercury passed through the total filter as a vapor.
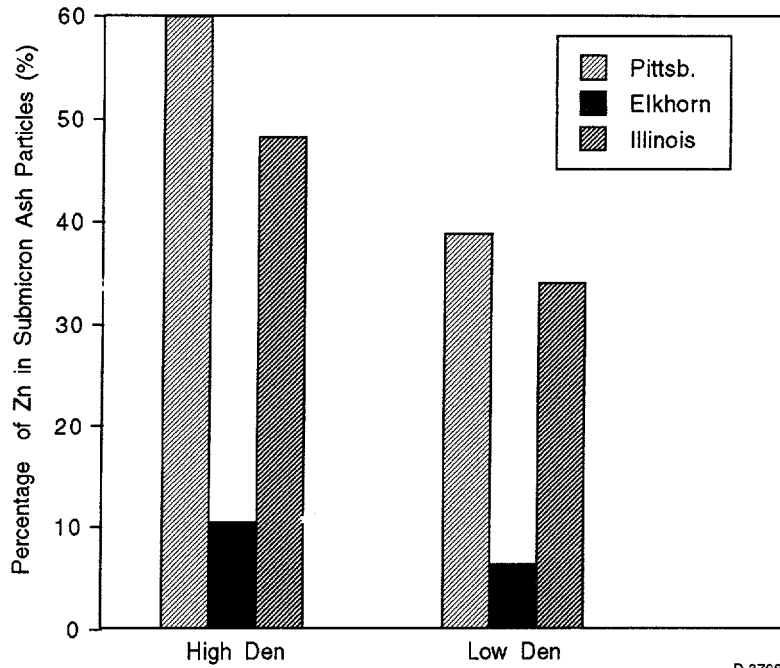
Figure 3-34. Zinc vaporization from 45 to 63 μm particles (MIT drop tube furnace).
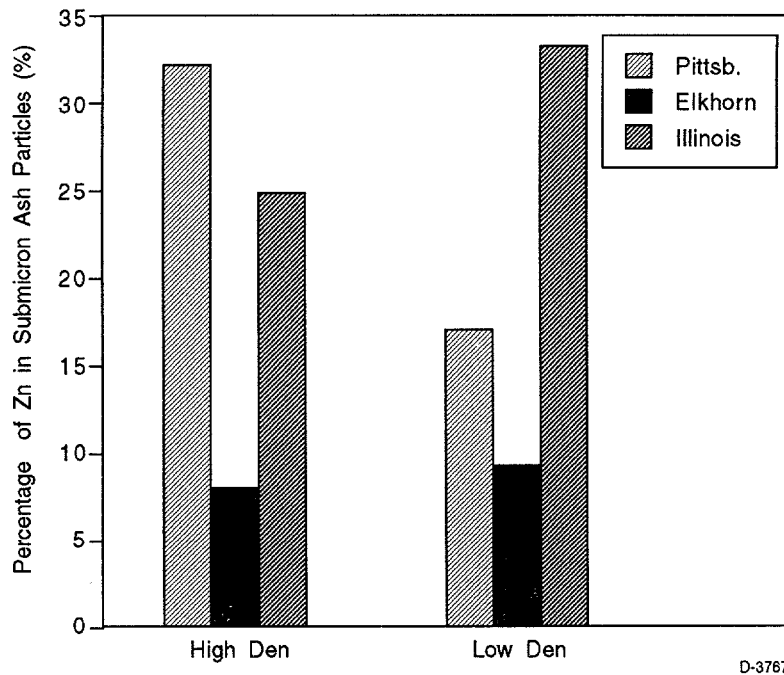
Figure 3-35. Zinc vaporization from 90 to 106 μm particles (MIT drop tube furnace).
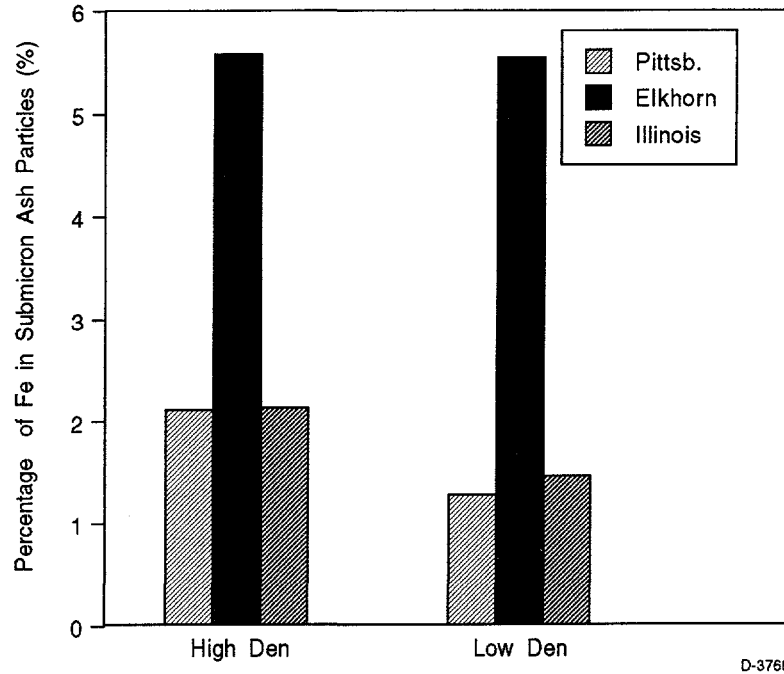
Figure 3-36. Iron vaporization from 45 to 63 µm particles (MIT drop tube furnace).
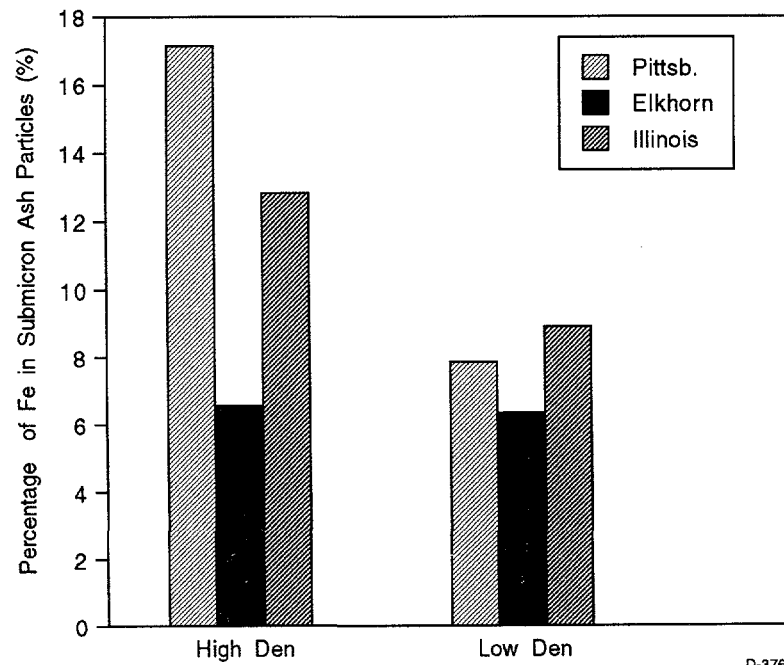
Figure 3-37. Iron vaporization from 90 to 106 µm particles (MIT drop tube furnace).
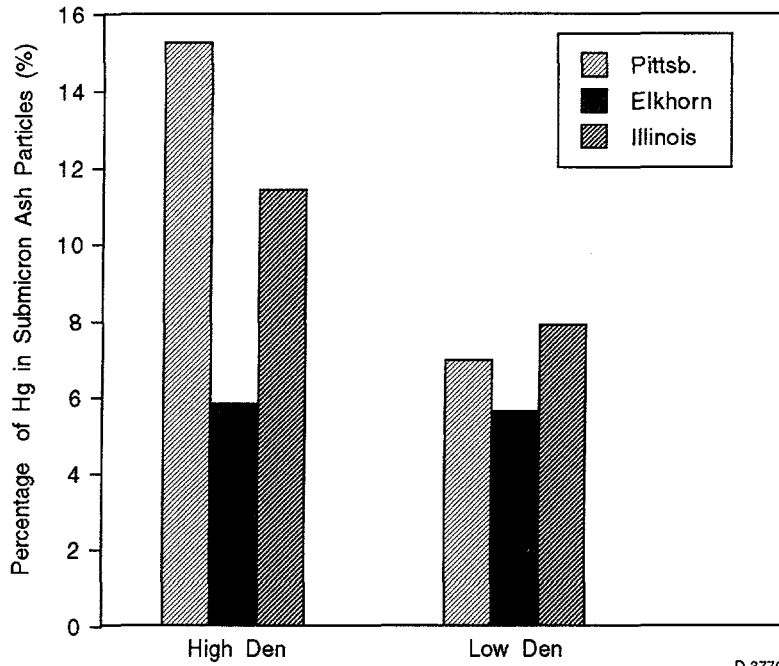
Figure 3-38. Mercury vaporization from 45 to 63 μm particles (MIT drop tube furnace).
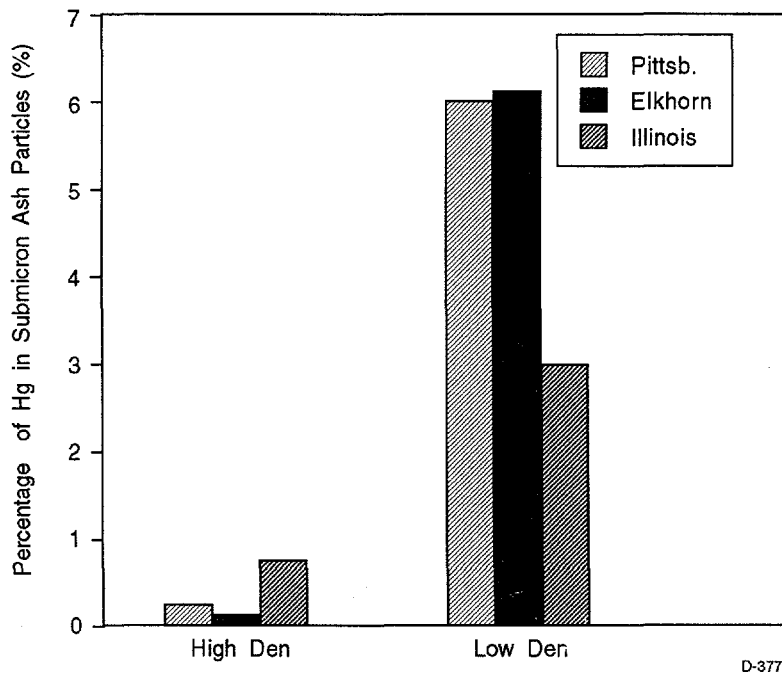
Figure 3-39. Mercury vaporization from 90 to 106 μm particles (MIT drop tube furnace).

Chromium

Cr XANES analysis has been performed on ash samples prepared from size and density segregated fractions of the Pittsburgh #8 coal. The spectra are shown in Figure 3-40. A detailed discussion of these data will be attempted in a subsequent report; in this report, we will only note the lack of change of the oxidation state of chromium in these samples, despite the variation in ash-particle size and atmosphere to which these samples have been subjected.
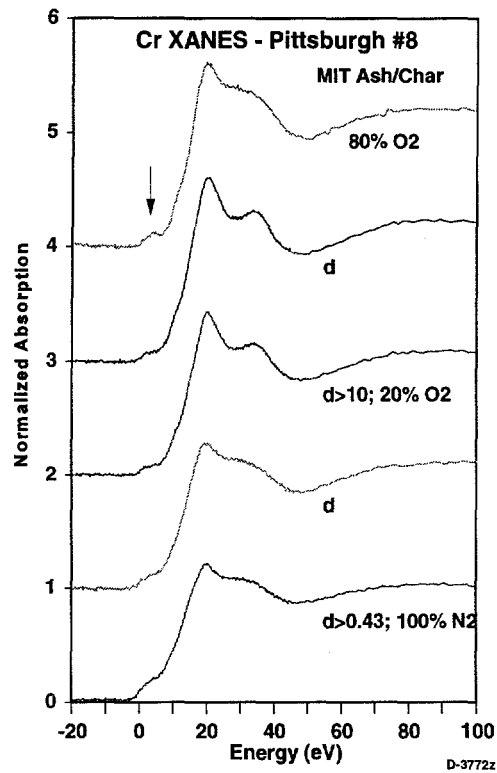
Figure 3-40. Chromium XANES spectra for ash samples of Pittsburgh coal (MIT drop tube furnace).

The oxidation state of chromium appears to be almost entirely Cr^{3+} in all samples; this is indicated by the small size and broad appearance of the pre-edge peak (denoted by the arrow in Figure 3-9) in all samples. If significant Cr(VI) were present in these samples, the pre-edge peak would occur as a sharp peak at about 4 eV and the intensity would increase with increasing Cr(VI), until at 100% Cr(VI), it would be of comparable height to the edge-step.

3.4   Post-Combustion Transformations (UA)

During the past quarter, the design for the mercury adsorption apparatus was completed and construction of the apparatus is underway. Upon receipt of char samples from the selected coals, we will begin testing the Hg sorption properties of each char. The reactor is shown in Figure 3-41.

3-40

1. Nitrogen   2. Air   3. Water Saturator
4. Hg Source   5. Reactor   6, 7. Activated Carbon Columns   D-3804
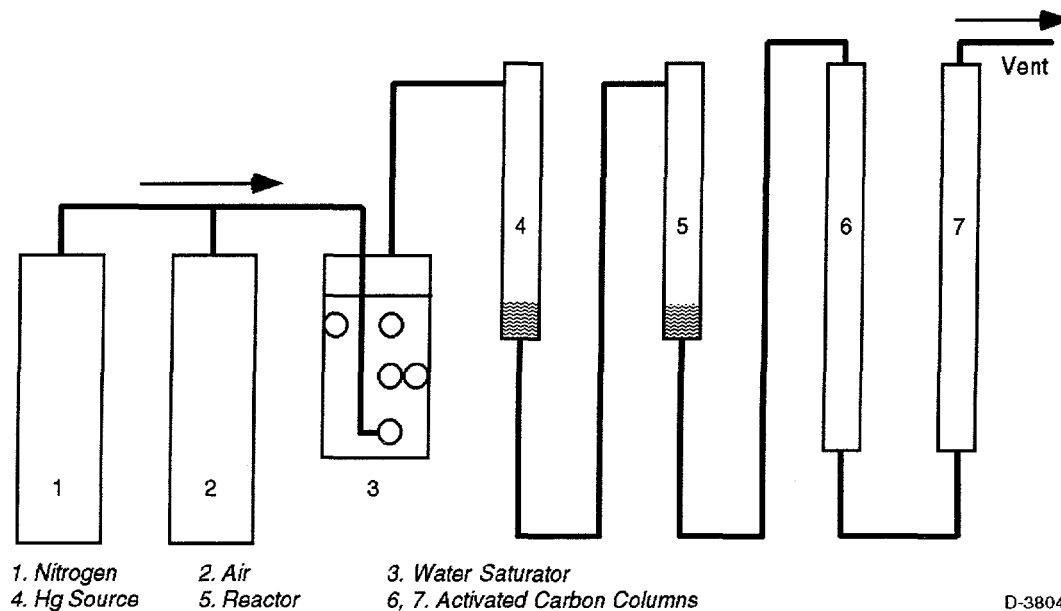
Figure 3-41. Schematic diagram of experimental apparatus.

The apparatus consists of major sections: gas preparation, sorption reactor, and an exhaust cleanup section. In the gas preparation section (items 1 through 4 in Figure 3-41), a simulated flue gas is prepared containing 15% CO_2, 2% O_2, 3% water, and the balance N_2. This gas then passes through the fixed temperature mercury source to achieve the desired gas phase mercury content. The temperature of the source reactor and the sorption reactor are held constant by using a temperature controller. The mercury-laden gas then passes through the sorption reactor, which contains the char, and is passed through two chambers filled with activated carbon. These chambers remove the mercury before the gas is exhausted into a hood.

The concentration of mercury in the gas phase will be calibrated by two methods. One is the direct weighting method. The weights of the mercury source before and after experiment are measured by an analytical balance with up to four digit accuracy. The gas concentration is then calculated by using this weight difference and the gas flow rate. The second method is atomic adsorption. The source is placed in the source reactor, and SFG passed through the system. As no sorbent will be placed in the sorption reactor, all the mercury will be captured by the exhaust section. A sample of the carbon from the exhaust section will be analyzed. Based on the mercury concentration in the carbon, and the total gas passed through the bed, it will be possible to estimate the mercury concentration in the gas.

3.5   Organic Emissions (Princeton) and Model Validation (UConn)

A preliminary analysis of the organic and trace element emissions data in the literature was completed in the last quarter. A report on these results was prepared and is currently under review by the Electric Power Research Institute (EPRI). This report will be presented in the next quarterly report.

3.6   Model Development (PSI)

One of the primary modeling tasks in Phase I is to determine whether equilibrium models can be used to predict the partitioning of metals in the flue gas. If equilibrium is a valid assumption for a particular element, then predicting the fate of the element is relatively straightforward. On the other hand, if equilibrium will not be attained in the flue gas, kinetic models may have to be developed in the Phase II program.

What makes us suspect that equilibrium will not be attained in the flue gas? The flue gas in a coal-fired power plant cools rapidly as heat is transferred to water and steam. Figure 3-42 shows a typical time-temperature history in a coal-fired power plant. Minor species in the flue gas such as CO and SO_2 do not have time to equilibrate as the gas cools. For example, the oxidation of SO_2 to SO_3 in coal combustion flue gas does not proceed at a fast rate below about 1500 K[13] and thus the SO_3 concentration is effectively frozen below this temperature in the flue gas. Similarly for trace species, present in ppm or ppb amounts, equilibrium may not be attained as the flue gas cools.
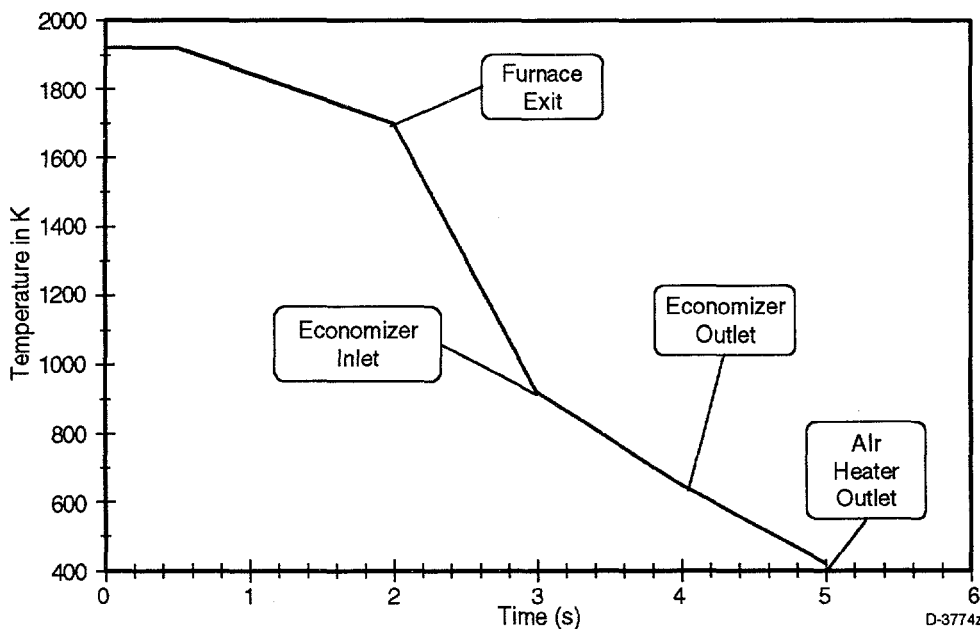
Figure 3-42. Time-temperature history for pulverized coal-fired boiler.

We begin our examination of the validity of equilibrium with mercury. This element stands apart from the other trace metals in coal because it is very volatile in the flue gas and because it does not interact with the bulk ash constituents. Equilibrium calculations were conducted using SOLGASMIX. The thermochemical database in the HSC package provided thermochemical data on the species of interest. Calculations were carried out for all four program coals using the material balances in Table 3-10. The species used were as follows:

Gas: CO, CO_2, Cl_2, H_2, HCl, H_2O, Hg, $HgCl_2$, HgO, N_2, NO, NO_2, O_2, SO_3

Condensed: C, Hg, HgO, $HgSO_4$

3-42

Table 3-10. Compositions for Equilibrium Calculations at SR = 1.2

	Elkhorn/Hazard	Pittsburgh	Illinois 6	Wyodak (1)
Ultimate Analysis (wt%)				
H	4.85	4.98	5.1	7.04
C	74.87	76.62	67.7	52.84
N	1.43	1.48	1.18	0.7
S	0.82	1.64	3.6	0.39
O	10.45	8.19	12.14	34.54
Ash	7.41	7.01	10.26	4.49
Minor Species (ppm)				
Cl	1700	980	340	550
Hg	0.13	0.11	0.11	0.11
Gas Composition at SR = 1.2 (in vol%)				
CO_2	14.5	14.44	14.26	13.86
H_2O	5.7	5.69	6.51	11.13
O_2	4.13	3.86	4.21	6.27
N_2	76.49	76.59	75.8	72.17
(in ppm)				
SO_2	594	1166	2837	383
HCl	111	62	24	49
Hg	0.0015	0.00124	0.0014	0.00172
SO_3 (2)	8.2	15.5	39.6	6.5

(1) Wyodak analysis from previous program
(2) Based on kinetics at 1400 K

The equilibrium between SO_2 and SO_3 was frozen in these calculations. Without this assumption, all the sulfur is predicted by the equilibrium calculations to exist as SO_3 at low temperatures. This result is contrary to observations from power plants. The concentration of SO_3 in the flue gas was set equal to that predicted at 1400 K based on kinetic arguments.[14]

The results, broadly, are as shown in Figure 3-43. Below 725 K (450°C) all the Hg is predicted to exist as $HgCl_2$. Below about 425 K (150°C) condensation of $HgSO_4$ is predicted. However, this temperature is below the acid dewpoint of the flue gas. The complex aqueous phase chemistry that occurs in the flue gas below this temperature is not included in the calculation. Thus, we won't consider the equilibrium calculation to be valid below the acid dewpoint.
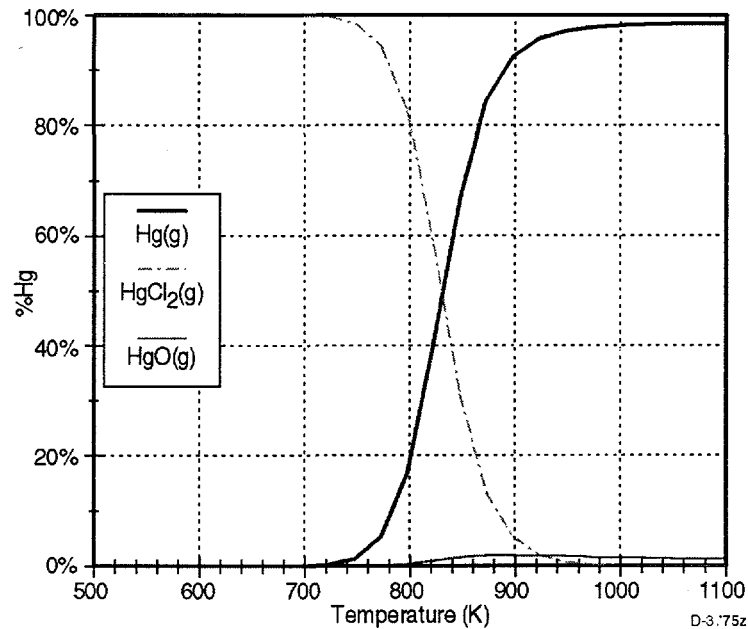
Figure 3-43.   Equilibrium mercury speciation in flue gas as a function of temperature (Pittsburgh coal).

Above about 975 K (700°C) 99% of the Hg is predicted to exist as gaseous Hg. The rest (1%) is predicted to be gaseous HgO. Between 725 and 975 K, the split between $HgCl_2$ and Hg is determined by the chlorine content of the coal (via the HCl content of the gas). HCl concentrations in the gas are predicted to be in the range of 24 to 111 ppm for the program coals. Even at these low concentrations, the reaction between Hg and HCl dominates the equilibrium chemistry. The temperature at which half the mercury exists as Hg (Figure 3-44) is strongly dependent on the chlorine content of the coal.

How do the equilibrium calculations compare with measured speciation from pilot and field sampling? As cited by Galbreath and Zygarlicke,[15] about half the mercury is found as Hg(g) before the APCD. The rest is almost always oxidized mercury species. After the ESP, the proportions are about the same. After the FGD, however, about 75% of the mercury is found as Hg(g).
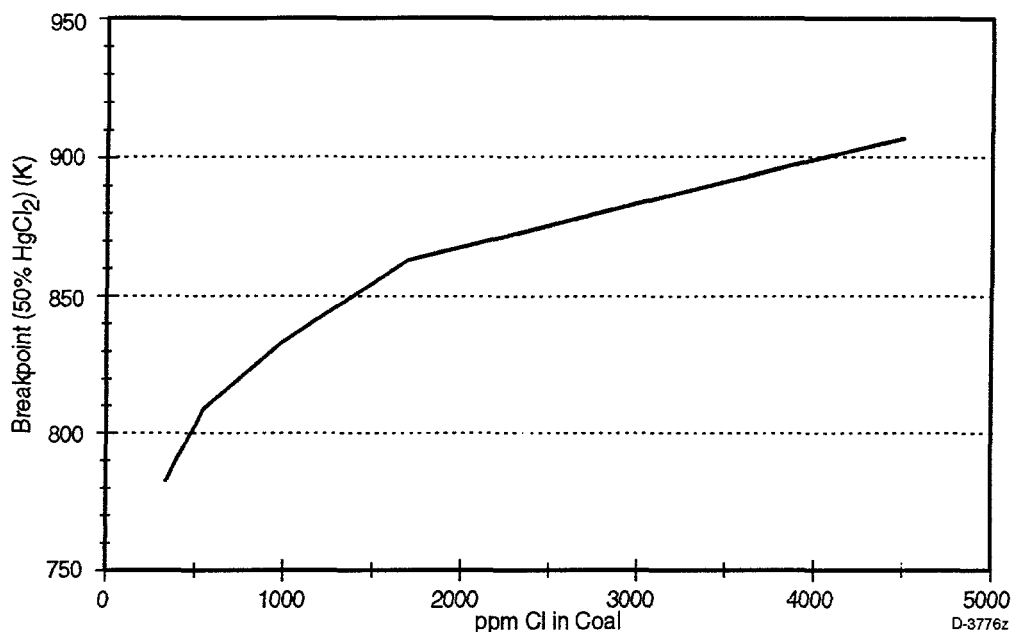
Figure 3-44. Equilibrium mercury speciation in flue gas: temperature of 50% $HgCl_2$ in gas.

Since equilibrium predicts all the Hg as gaseous $HgCl_2$ at low temperatures, how can we explain the field data? The answer to this question is important because, ultimately, we want to be able to predict the speciation of mercury at the air heater exit. The efficiency of removal of mercury in scrubbers and spray dryers is higher for $HgCl_2$ than Hg. Evidence also suggests that $HgCl_2$ is more easily removed by activated carbon and/or char than is elemental Hg.

There is some evidence from laboratory and pilot data that the kinetics of Hg oxidation are slow at low temperatures. Based on pilot data, the addition of HCl at temperatures below 450 K (180° C) did not increase the amount of $HgCl_2$ in coal combustion flue gas, indicating no reaction at those temperatures.[15] In laboratory experiments[16] using simulated flue gas (in the presence of activated carbon), equilibrium was not attained for Hg at temperatures below 473 K (200°C).

Since a substantial amount of elemental Hg is found in coal combustion flue gas and equilibrium does not predict any Hg below 725 K, it is reasonable to conclude that the kinetic limitation on oxidation of Hg occurs at some temperature between 725 and 975 K. As discussed above, there are other combustion species that are kinetically limited in this way.

We can propose an hypothesis for mercury speciation in coal combustion flue gas which states that the Hg equilibrium is frozen below some temperature between 725 and 975 K. If we assume that the time-temperature history is similar for most power plants, then the temperature at which mercury speciation is fixed will depend on the chlorine content of the coal. As Figure 3-44 indicated, chlorine content has strong effect on the equilibrium distribution as a function of temperature. In order to test the hypothesis, data on mercury speciation in flue gas and on coal chlorine content are needed. Field data reported in the open literature on mercury speciation do not usually include coal chlorine content.

3-45

Tumati and DeVito[17] conducted pilot scale testing of a Pittsburgh coal and an Illinois 6 coal in which the chlorine and mercury contents of the coal were reported as well as mercury speciation in the flue gas. The mercury speciation results are compared with equilibrium predictions in Figure 3-45. The percentage of mercury as $HgCl_2$ is plotted as a function of coal chlorine content. The lines indicate hypothetical temperatures at which the equilibrium is frozen. The pilot data are consistent with a cut-off temperature for mercury oxidation of approximately 850 K. Three field data points taken from the DOE-sponsored field sampling program[18-20] are also shown. These indicate higher proportions of $HgCl_2$ (or, a lower temperature for frozen equilibrium). Further work will be required to gather field data (particularly from the PISCES database) to provide a stronger validation of this hypothesis.
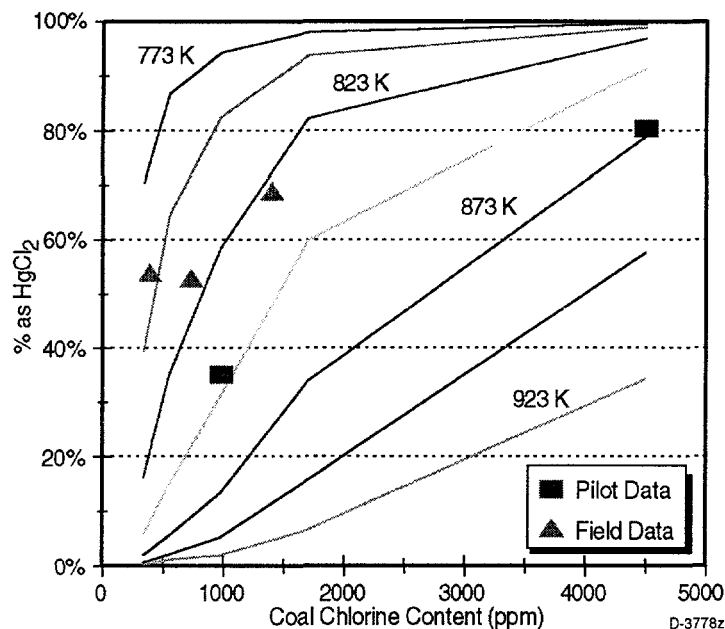
Figure 3-45. Mercury speciation as a function of coal chlorine content: theoretical predictions compared with pilot scale data from references 16 to 19.

SECTION 4

CONCLUSIONS

4. CONCLUSIONS

The results discussed in the previous section demonstrate that PSI and team members were able to take great strides in the last quarter toward a better understanding of both the form of occurrence of trace elements in coal and their vaporization behavior during combustion. Various techniques, such as XAFS and electron-microprobe, were utilized to determine the chemical forms of the trace elements in the programs coals, and trace element-mineral associations in these coals. Although the work is still ongoing, it has led to an interesting observation for arsenic. Arsenic was found to be primarily arsenical pyrite (arsenic substitutes for sulfur in the pyrite matrix) in the Pittsburgh and Illinois No. 6 coals. However, approximately 30% of the arsenic was found to be in the oxidized form (arsenate) in the Elkhorn/Hazard coal. The forms of iron (from Mössbauer analysis) indicated that a significant amount of jarosite (an iron sulfate mineral) was present in the Elkhorn/Hazard coal, but not in the other two coals. These results suggest that the arsenic initially associated with pyrite oxidizes to arsenate as the pyrite weathers. Thus, the fraction of oxidized arsenic (which may be approximated using the form of sulfur analysis) may be correlated with the fraction of oxidized pyrite. This may be an important method for estimating the fraction of oxidized arsenic, which may have a different vaporization behavior, in a given coal. To test this hypothesis, a controlled low temperature coal oxidation experiment (to simulate weathering), coupled with combustion testing of the 'weathered' coal, is underway.

The combustion testing performed in last quarter also yielded some interesting conclusions. Antimony, arsenic, and selenium were found to be enriched in the small ash particles during combustion testing of two utility grind coals and several size and density fractionated coal samples, suggesting that vaporization is significant during combustion. However, a significantly higher vaporized fraction was noted for the MIT facility as compared to the PSI facility. The MIT experiments provide a measure of the total element that is released into the vapor phase. The PSI facility, on the other hand, provides a measure of the *net* vaporization in the flame zone. Therefore significant differences in the measured fractional vaporization between the two facilities may suggest post-vaporization capture in the flame zone. This phenomenon will continue to be explored in the next quarter.

SECTION 5

REFERENCES

5. REFERENCES

1. Bool, III, L.E., Senior, C.L., Huggins,F., Huffman, G.P., Shah, N., Wendt, J.O.L., Sarofim, A., Olmez, I., and Zeng, T., "Toxic Substances from Coal Combustion -- A Comprehensive Assessment," Quarterly Report No. 3 prepared for Department of Energy, PETC, under Contract No. DE-AC22-95PC95101, PSIT-1245, July (1996).

2. ASTM (American Society for Testing and Minerals), Annual Book of ASTM Standards, Vol. 5.05 Gaseous Fuels, Coal and Coke, p. 526, Philadelphia, PA (1993).

3. Pontolillo, J. and Stanton, R.W., "Coal petrographic laboratory procedures and safety manual II," *U. S. Geological Survey Open-File Report 94-631*, p. 69 (1994).

4. Finkelman, R.B., "Modes of occurrence of potentially hazardous elements in coal: Levels of confidence," *Fuel Processing Technology* **(39)**, 21-34 (1994).

5. Palmer, C.A., Krasnow, M.R., Finkelman, R.B., and D'Angelo, W.M., "An evaluation of leaching to determine modes of occurrence of selected toxic elements in coal," *Journal of Coal Quality* **12**(4), 135-141 (1993).

6. Finkelman, R.B. Palmer, C.A., Krasnow, M.R., Aruscavage, P.J. Sellers, G.A., and Dulong, F.T., 1990, "Combustion and leaching behavior of elements in Argonne Premium Coal Samples," *Energy and Fuels* **4**(5), 755-766 (1990).

7. F. E. Huggins, N. Shah, J. Zhao, F. Lu, and G. P. Huffman, "Nondestructive determination of trace element speciation in coal and ash by XAFS spectroscopy," *Energy & Fuels* **7**(4), 482-489 (1993).

8. G. P. Huffman, F. E. Huggins, N. Shah, and J. Zhao, "Speciation of arsenic and chromium in coal and combustion ash by XAFS spectroscopy," *Fuel Proc. Technol.* **39**, 47-62 (1994).

9. F. E. Huggins, and G. P. Huffman, "Application of XAFS spectroscopy to coal geochemistry," *Geochim. Cosmochim. Acta (R. G. Burns, Mem. Vol.)*, in press (1996).

10. F. E. Huggins, et al., work in progress.

11. Bool, L.E., and Helble, J.J., "A Laboratory Study of the Partitioning of Trace Elements During Pulverized Coal Combustion," *Energy & Fuels* **(9)**, 880-887 (1995).

12. Bool, L.E., Peterson, T.W., Wendt, J.O.L., "The Partitioning of Iron During the Combustion of Pulverized Coal," *Combustion and Flame* **(100)**, 262-270 (1995).

13. F. E. Huggins, and G. P. Huffman, "Chlorine in coal: an XAFS spectroscopic investigation," *Fuel* **74**, 556-569 (1995).

14. Flagan, R.C and Seinfeld, J. H, <u>Fundamentals of Air Pollution Engineering</u>, pp.217-219, Prentice Hall: Englewood Cliffs, NJ (1988).

15. Galbreath, K.C and Zygarlicke, C.J. "Mercury Speciation in Coal Combustion and Gasification Flue Gases," *Env.Sci.Tech.* **30,** 2421-2426, (1996).

16. Nordin, A., Schager, P., and Hall, B. "Mercury Speciation in Flue Gases: A Comparison of Results from Equilibrium Calculations with Results from Laboratory Experiments," presented at Finnish Flame Days meeting.

17. Tumati, P.R. and DeVito, M.S. "Partitioning Behavior of Mercury During Coal Combustion," ASME Paper 93-JPGC-EC-8, presented at the Joint ASME/IEEE Power Generation Conference, Kansas City, 1993.

18. Radian Corporation, "A Study of Toxic Emissions from a Coal-Fired Power Plant Utilizing and ESP While Demonstrating the ICCT CT-121 FGD Project," Final Report on Contract DE-AC22-93PC93253, 1994.

19. Southern Research Institute, "Characterizing Toxic Emissions from a Coal-Fired Power Plant Demonstrating the AFGD ICCT Project and a Plant Utilizing a Dry Scrubber/Baghouse System," Final Report on Contract DE-AC22-93PC93254, 1994.

20. Roy F.Weston, Inc., "Toxic Assessment Report Illinois Power Company Baldwin Power Station - Unit 2," Final Report on Contract DE-AC22-93PC93255, 1994.

APPENDIX A

QUANTITATIVE MICROPROBE ANALYSES OF PYRITE GRAINS IN THE PITTSBURGH, ELKHORN/HAZARD, AND ILLINOIS NO. 6 COALS

Appendix A. Quantitative Microprobe Analyses of Pyrite grains in the Pittsburgh, Elkhorn/Hazard, and Illinois No. 6 coals

Pittsburgh Coal

Analysis	Date (1996)	Pellet	Morphology of pyrite	Size (μm)	Total (wt.%)	As (wt.%)	Ni (wt.%)	Cu (wt.%)
1.1	9-12	C	irreg.	25	97.91	0.121	0.011	0.021
7.2	9-12	C	irreg.	25	99.09	0.134	0	0
8.1	9-12	C	subh.	30	97.26	0.129	0	0.022
8.2	9-12	C	subh.	30	99.73	0.178	0	0.033
8.3	9-12	C	subh.	30	99.96	0.178	0	0.024
9.2	9-12	C	subh.	20	97.24	0.127	0.005	0
10.1	9-12	C	subh.	50	95.2	0.08	0.003	0
10.2	9-12	C	subh.	50	96	0.116	0	0.01
10.3	9-12	C	subh.	50	95.36	0.097	0.007	0.009
11.2	9-12	C	euh.	10	100.3	0.135	0	0
12.1	9-12	C	subh.	25	96.57	0.115	0	0.003
12.2	9-12	C	subh.	25	98.04	0.094	0.005	0.002
12.3	9-12	C	subh.	25	97.93	0.112	0	0
12.4	9-12	C	subh.	25	98.37	0.124	0	0
14.1	9-12	C	elong.	50	96.33	0.144	0.008	0
14.2	9-12	C	elong.	50	97.28	0.144	0	0
14.3	9-12	C	elong.	50	100.13	0.152	0.003	0
1.3	9-26	B	irreg.	60	95.25	0.113	0.002	0
3.1	9-26	B	subh.	20x20	98.11	0.053	0.006	0.096
3.2	9-26	B	subh.	20x20	99.82	0.07	0	0.109
4.2	9-26	B	subh.	20x60	100.44	0.045	0	0
4.3	9-26	B	subh.	20x60	100.36	0.024	0	0
5.1	9-26	B	subh.	40x60	99.57	0.082	0	0
5.2	9-26	B	subh.	40x60	100.09	0.042	0	0
5.3	9-26	B	subh.	40x60	99.85	0	0	0
9.1	9-26	B	subh.	100x130	95.83	0	0.001	0.011
9.2	9-26	B	subh.	100x130	97.37	0.065	0.002	0
9.3	9-26	B	subh.	100x130	98.61	0.018	0	0.007
9.4	9-26	B	subh.	100x130	99	0.056	0.013	0.001
9.5	9-26	B	subh.	100x130	97.62	0.026	0	0.022
10.1	9-26	B	subh.	30x40	100.12	0.064	0	0.004
10.2	9-26	B	subh.	30x40	99.04	0.038	0	0.022
11.1	9-26	B	framb.	20	96.12	0.055	0.018	0.008
12.1	9-26	B	euhed.	10	96.46	0.062	0.006	0.04
13.1	9-26	B	subh.	15x20	97.46	0.05	0.012	0
14.1	9-26	B	subh.	15x40	98.79	0.118	0	0.036
14.2	9-26	B	subh.	15x40	98.45	0.089	0	0.014
15.1	9-26	B	subh.	10x30	98.72	0.056	0.003	0.004

Elkhorn/Hazard Coal

Analysis	Date	Pellet	Morphology of pyrite	Size (μm)	Total (wt.%)	As (wt.%)	Ni (wt.%)	Cu (wt.%)
1.1	9-12	C	irreg.	50	96.83	0.234	0	0
1.2	9-12	C	irreg.	50	96.39	0.186	0	0
8.1	9-12	C	subh.	40	97.1	0.171	0	0
8.2	9-12	C	subh.	40	97.73	0.219	0.001	0.007
8.3	9-12	C	subh.	40	96.7	0.162	0	0.003
11.3	9-12	C	round	80	95.17	0.373	0	0.014
11.4	9-12	C	round	80	97.09	0.226	0.01	0
11.5	9-12	C	round	80	97.55	0.186	0.015	0.007
11.6	9-12	C	round	80	97.22	0.336	0.015	0.02
2.1	9-26	B	subh/euh.	30x50	98.85	1.799	0.002	0.002
2.2	9-26	B	subh/euh.	30x50	98.71	1.971	0	0.006
2.3	9-26	B	subh/euh.	30x50	98.66	2.1	0	0
4.1	9-26	B	euh.	30x40	100.11	0.057	0.001	0
4.2	9-26	B	euh.	30x40	99.87	0.048	0.007	0.006
8.1	9-26	B	euh.	35x40	95.52	0.113	0.013	0.038
11.1	9-26	B	subh.	40x50	96.35	0.118	0.003	0.044
11.2	9-26	B	subh.	40x50	96.39	0.23	0.012	0.048
12.1	9-26	B	round	45	96.59	0.122	0	0
12.2	9-26	B	round	45	96.2	0.04	0.01	0.022
12.3	9-26	B	round	45	96.33	0.036	0.01	0.005
14.1	9-26	B	round	25	99.16	0.081	0.061	0.01
14.2	9-26	B	round	25	99.2	0.012	0.052	0.016

Illinois #6 Coal

Analysis	Date	Pellet	Morphology of pyrite	Size (μm)	Total (wt.%)	As (wt.%)	Ni (wt.%)	Cu (wt.%)
1.1	9-12	C	subh.	50	95.45	0.063	0	0.002
1.2	9-12	C	subh.	50	96.22	0.077	0	0.013
10.1	9-12	C	subh.	50	101.61	0.059	0	0
10.2	9-12	C	subh.	50	101.52	0.135	0	0
10.3	9-12	C	subh.	50	101.5	0.164	0	0
3.1	9-26	B	euh.	20x65	99.04	0.104	0	0
3.2	9-26	B	euh.	20x65	99.52	0.128	0.001	0.011
3.3	9-26	B	euh.	20x65	99.1	0.156	0	0
4.1	9-26	B	euh.	20x20	98.91	0.076	0.002	0
6.1	9-26	B	subh.	30x100	101.2	0.031	0.003	0
6.2	9-26	B	subh.	30x100	100.37	0.039	0	0.002
6.3	9-26	B	subh.	30x100	100.68	0.052	0	0
6.4	9-26	B	subh.	30x100	99.69	0.057	0.009	0.015
8.1	9-26	B	framb.	15	96.74	0.087	0.262	0.044
11.1	9-26	B	subh.	70x40	100.52	0.062	0	0
11.2	9-26	B	subh.	70x40	100.85	0.094	0	0.003
12.1	9-26	B	framb.	20	98.65	0.037	0.009	0
13.1	9-26	B	euh.	40	100.44	0.006	0.003	0.016
13.2	9-26	B	euh.	40	100.71	0.055	0.004	0.007
14.1	9-26	B	framb.	10	96.39	0.083	0.095	0.039
15.1	9-26	B	subh.	20x70	99.83	0.015	0.001	0
15.2	9-26	B	subh.	20x70	100.35	0.081	0.004	0.007
15.3	9-26	B	subh.	20x70	101.19	0.068	0.006	0